

SCHOOL OF SCIENCE

Department of Industrial Chemistry “Toso Montanari”

Second cycle degree in

**Low Carbon Technologies and Sustainable
Chemistry**

Classe LM-75 - Scienza e Tecnologie per l’Ambiente e il Territorio

Investigation of Aqueous Phase Reforming
reaction of xylitol over multifunctional
heterogeneous catalysts

Experimental degree thesis

CANDIDATE

Yubing Chen

SUPERVISOR

Chiar.mo Prof. Fabrizio Cavani

CO-SUPERVISOR

Dr. Tommaso Tabanelli

Federico Bugli

Dr. Andrea Fasolini

Project developed in the laboratory of the “Catalysis for renewable and innovative processes” Group of the Department of Industrial Chemistry “Toso Montanari”

University of Bologna (Italy)

Table of Contents

Abstract	6
Acknowledgment	7
Abbreviation list	8
1 INTRODUCTION:.....	1
1.1 Energy situation:	1
1.2 Biorefinery.....	3
1.2.1 “Lignin first” approach	6
1.2.2 Aqueous Phase Reforming (APR)	8
1.2.3 Thermodynamic and kinetic considerations.....	11
1.2.4 Catalyst for APR reaction.....	13
1.2.5 APR feedstocks alternatives.....	16
1.2.6 Mechanism of APR reaction.....	18
2 THESIS SCOPE.....	21
3 EXPERIMENTAL PART:	22
3.1 Specific reactor.....	22
3.1.1 Reaction procedure	23
3.2 Catalysts synthetic procedures.....	24
3.2.1 Synthesis of magnesium oxide (MgO).....	24

3.2.2	Synthesis of Magnesium/Aluminum mixed oxide (MgAlOx)	25
3.2.3	Synthesis of Pt- supported catalysts	26
3.3	Gas phase analysis	26
3.4	Liquid phase analysis	27
3.5	Calculations	28
3.6	Catalyst Characterization	30
3.6.1	X-ray diffraction analysis (XRD)	30
3.6.2	Brunauer-Emmett-Teller analysis (BET)	32
3.6.3	Description of CO ₂ -TPD, NH ₃ -TPD and TPR	32
3.6.4	Microwave plasma-atomic emission spectroscopy (MP-AES)	34
3.6.5	Thermal gravimetric analysis (TGA)	34
3.7	Chemicals	35
4	RESULTS AND DISCUSSION:	35
4.1	Magnetic catalysts: 5%wt Pt/ γ -Fe ₂ O ₃	35
4.2	Pt supported over metal oxide supports	40
4.3	Catalyst Characterization	41
4.4	Catalytic test	42
4.4.1	5%wt Pt/Al ₂ O ₃	42
4.4.2	Comparison between different metal oxide supported catalyst	43

4.4.3	Reaction mechanism investigation.....	44
4.4.4	Optimization of the reaction condition with Pt/MgAlOx.....	50
4.4.4.1	Spent catalyst characterization.....	54
4.4.4.2	Recycle test.....	56
5	CONCLUSION:	65
6	REFERENCE:.....	66

Abstract

The present work is focused on the study of aqueous phase reforming reaction (APR) of xylitol, a polyol obtainable from the hemicellulose fraction of lignocellulosic biomass. The APR mechanism as well as the relation within catalyst activity and metal/support properties has been investigated and discussed by changing the main operating conditions (e.g. reaction temperature and time). Interestingly, dedicated test performed by feeding glycerol solutions have underlined the crucial role of preliminary retro-aldol reactions on the xylitol APR which indeed led to glyceraldehyde and glycolaldehyde, both obtained from glycerol as well, which lead to similar products distributions after the catalytic tests. A number of catalysts were evaluated, with interesting results, in terms of H₂ yield obtained with polyfunctional material based on supported Pt. Catalyst stability was investigated by recyclability tests and dedicated analysis of the dissolved metals in solution. In this way the most promising catalyst showed to be stable for at least 3 cycles of reaction without any need of intermediate regeneration procedures or usage of harsher reaction conditions.

Acknowledgment

This thesis is the culmination of a long and arduous journey-one that I have only been able to make as a result of the dedicated support I have received from so many people along the way.

The deepest and sincerest gratitude goes to my supervisor Professor Cavani, Tabanelli, Fasolini, and my little boss Bugli for their continuous and invaluable guidance throughout my research. It is a great honor and privilege that I was given the opportunity to work under this group. I would like to thank them for their patience, support, empathy and great sense of humor. In addition, I am also thankful to the academics and colleagues in the laboratory of the "Catalysis for renewable and innovative processes" Group of the Department of Industrial Chemistry "Toso Montanari". I would also like to thank my external and internal examiners for their valuable comments which helped in improving the quality of the thesis. I would gratefully acknowledge the support of my dearest friends and research group mates for their encouragement, friendship and support since the beginning of my study. I am extremely grateful to my parents for their motivation, patience, love and care during my education and life journey. Without their help, this thesis would not have been accomplished. My final thanks go to all the people who have directly or indirectly supported me in completing my thesis. Sincere wishes to you may everything be pleasant and pleasant to you.

Abbreviation list

APR (Aqueous phase reforming)

WGS (Water gas shift)

SR (steam reforming)

BET (Brunauer-Emmett-Teller analysis)

H₂-TPR (H₂-Temperature programmed reduction)

TPD (temperature programmed desorption)

HPLC (high-performance liquid chromatography)

GC (Gas chromatography)

XRD (X-ray diffraction)

CB (Carbon balance)

EG (ethylene glycol)

LA (lactic acid)

MgAl-HT (MgAl- hydrotalcite)

MgAlO_x (MgAl mixed oxides)

MgAl-HTlcs (MgAl- hydrotalcite like compounds)

LDH (layered double hydroxide)

1 INTRODUCTION:

1.1 Energy situation:

Whenever humans enjoy convenience, the environment suffers. As a species we are all experiencing drastic climate change, which is the consequence of Greenhouse Gas (GHG) emissions caused by inconsiderate consumption of fossil fuels, especially for industrial production and transportation. Recently the scientific community acknowledged GHG emissions produced by fossil fuels as a primary cause of global warming.¹ To compensate this problem, there is an urgent need to change the energy supply system toward efficient and greener sources for sustainable development.

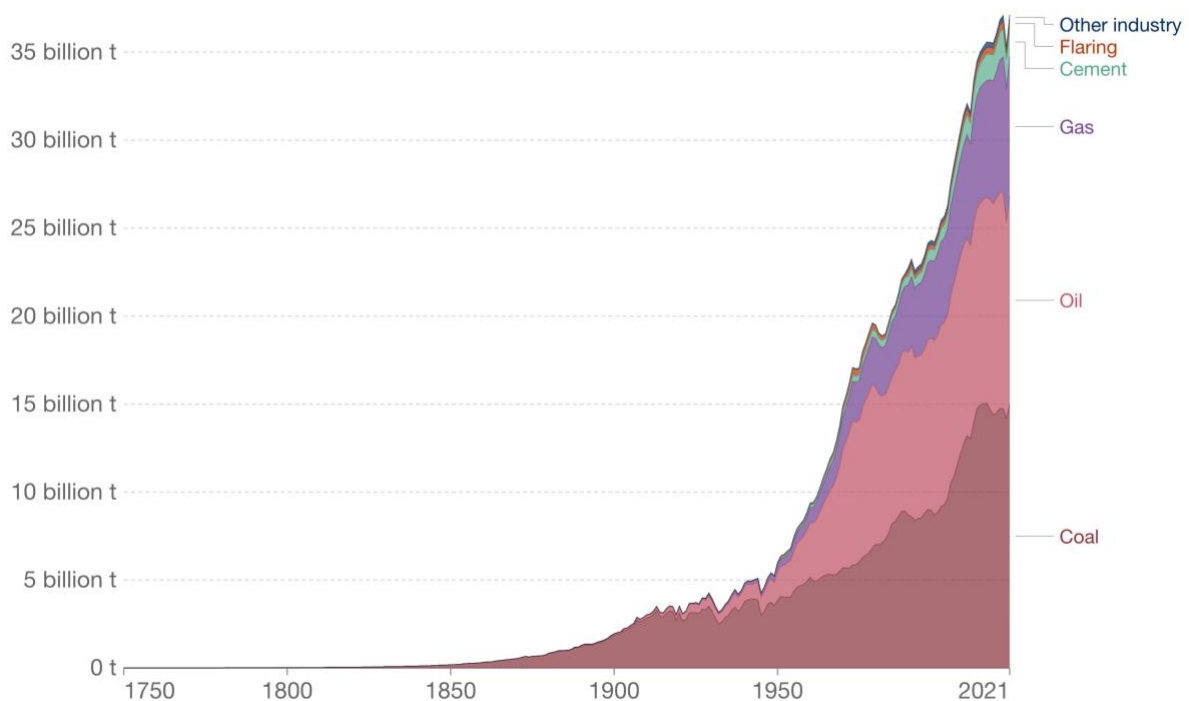


Figure 1 - Global CO₂ emissions of the main sources.²

Recently direct combustion has been partially replaced by electricity³, which is a secondary energy promising for a future energy system based on renewables but otherwise ineffective in a different scenario. A possible solution could be represented

by the use of hydrogen directly as a clean fuel or for the generation of electricity through fuel cells⁴. Currently, commercially available hydrogen is produced by different raw materials: natural gas, coal, and water. As reported in Figure 2, at the moment hydrogen production rely mainly on fossil fuels and the hydrogen extracted from renewable sources need further study and development.⁵ The hydrogen generation from fossil recourses is currently accomplished by steam reforming and partial oxidation mainly of methane, gasification of coal and oil and water hydrolysis.⁶

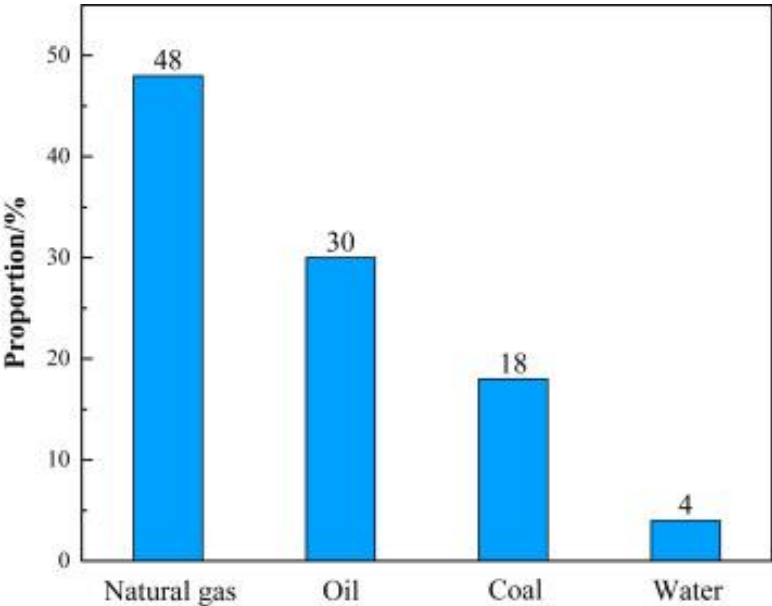


Figure 2 - Main feedstocks for current hydrogen production.⁷

Alternative routes are currently investigated by the scientific and industrial community to achieve sustainable hydrogen production which doesn't involve fossil fuels consumption or harsh conditions. In particular, water hydrolysis used solar or wind as driving force for renewable electricity may play a major role in the future together with alternative methods for the conversion of biomass, which absorb CO₂ during its lifetime, toward hydrogen and other added-value compounds, to achieve a net zero GHG emission.

1.2 Biorefinery

Biomass is material produced from the growth of microorganism, plants or animals. The most indicated type of biomass for these novel processes are lignocellulosic biomasses. During the growth process of a plant, CO₂ is assimilated by the plant metabolism, which results in net zero emissions, which is a result of biomass assimilation. These feedstocks are complicated to process compared with petroleum because of their intrinsic characteristics, such as their moisture content, relatively low energy density, bulk density, morphology, and harvest time which may vary the composition of the biomass itself⁹. However, petroleum has a more predictable composition, and more importantly, it has been studied for decades, and massive facilities have already been established. To develop biorefinery processes, it is necessary to use facilities of a petroleum-like nature rather than changing the energy production system in a radical manner.

Scientists have developed energy crops that are capable of providing feedstocks that have a high growth rate and are suitable for cultivation on marginal and non-irrigated lands for the generation of energy and biofuels.¹⁰

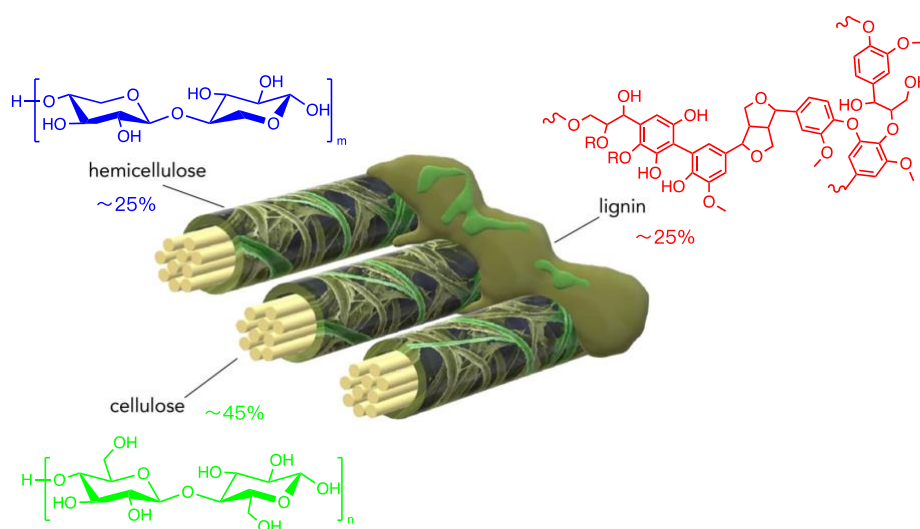


Figure 3 - Structure of lignocellulosic biomass. ^{11 12}

Raw lignocellulosic biomasses have different composition depending on the species, but the structural components could be summarized as:

- Hemicellulose, an amorphous and branched polymer consisting of monomers of C5 and C6 sugars such as xylose, arabinose, glucose, mannose, and galactose.
- Cellulose, a highly crystalline and linear polymer consisting of D-glucose units linked through glycosidic bonds in positions 1-4.
- Lignin, a branched polymer with a complex composition made up of phenolic units.

Figure 3 shows that the lignocellulose biomass is consist with cellulose, hemicellulose, lignin, and some other extractives. Cellulose and hemicellulose are polysaccharides that can be depolymerized into sugars, and further processed to get value-added products (bioethanol, biobutanol etc.) by various biological or chemical processes¹³. Lignin is bio-synthesized by the plant in the cell wall to provide mechanical resistance to support the polysaccharide ¹⁴, it's complicated structure and refractoriness represent a limit for its valorization.

A network of facilities which incorporates equipment and processes for converting biomass into transportation biofuels, electricity, and chemicals is known as a biorefinery.¹⁵ The biorefinery concept embraces a vast range of technologies capable of integrate biomass conversion processes and equipment to produce biofuels, energy, and chemicals from biomass. This concept is analogous to today's petroleum refinery, which produces multiple fuels and products from petroleum.¹⁵ In this scenario, multiple bio-industries can integrate their material flows to fully utilize all biomass components: the waste from one bio-industry, such as lignin from a lignocellulosic biomass fractionation plant, becomes an input for other industries, resulting in integrated bio-industrial systems. Additionally, biomass resources are readily available locally in

many nations, and their use may help to lessen a country's reliance on imported fossil fuels.

Pretreatment of biomass

Biomass complex morphology makes them recalcitrant, complicating their use in bioconversion and bio-refinery processes¹⁶. In particular, biomass recalcitrance is closely related to the chemical and physical features of the plant cell wall; the presence of lignin, hemicellulose, pectin, ashes and their spatial interlinks are physical barriers to cellulose fibers preventing their degradation.⁹

Typically, biomass pretreatments are necessary to reduce the material recalcitrance enhancing cellulose availability. In general a pretreatment is designed to extract or degradate lignin to isolate the fraction containing carbohydrates, lower the crystallinity of cellulose and increase surface area and the porosity of the material (some of the most used are reported in Figure 4)¹⁷. These range of methods are comprehensive of both physical and chemical techniques which share in common harsh conditions and/or solvent usage.

Pretreatment methods	Advantages	Disadvantages	
Physical pretreatment	Mechanical splintered	Reduce particle size and cellulose crystallinity	Cannot remove lignin and hemicelluloses, high energy
	Microwave	Simple operation, energy-efficient, short time	High cost
	Ultrasonic	Improve accessibility and reactivity of cellulose	Negative to enzymatic hydrolysis
	High-energy electron radiation	Reduce cellulose polymerization degree	High cost
Chemical pretreatment	High-temperature pyrolysis	Decompose cellulose rapidly	Energy consumption, low productivity
	Concentrated acid	High sugar conversion	High toxic and corrosive, corrosive equipment, high cost
	Dilute acid	Fast and don not need recycle acid	High temperature and pressure, formation of inhibitors
	Alkali pretreatment	Room temperature, destroy lignin	Less sugar degradation
	Oxidation pretreatment	Environmental, remove lignin effectively	High cost,
	Organosolv pretreatment	Obtain pure lignin, cellulose and hemicelluloses	High cost, certain effects on environment and fermentation
Physicochemical pretreatment	Ionic liquid pretreatment	Environmental, large temperature range	High cost
	Steam explosion	Lignin transformation, hemicelluloses solubilization, Cost-effective	High temperature and pressure
	AFEX method CO ₂ explosion	increase surface area of cellulose, absence of inhibition substances formed	High cost, Not efficient for raw high lignin content material
Biological pretreatment	Electrical catalysis	Not produce inhibition compounds, cost-effective, Increases surface area, remove lignin effective	High pressure, do not affect lignin and hemicelluloses
	-	Cleanliness,	Lower efficient
		Degrades lignin and hemicellulose	Low rate of hydrolysis
		Low energy consumption	

Figure 4 -Summary of the main pre-treatments applicable to lignocellulosic biomass.¹⁷

The mentioned technologies are currently adopted for a biorefinery strategy mainly focus on the valorization of the fraction containing carbohydrates, leaving behind, as a

waste, the lignin fraction which is usually burned to recover some energy in the plant as a low quality fuel¹⁸. The valorization of lignin is moreover impeded by its degradation from “virgin” lignin to “technical” lignins, characterized by the formation of new C-C bonds, which occurs in the harsh conditions imposed by pretreatments, in fact the C-O-C etheral bonds which characterize the lignin polymer are cleaved at the pretreatment’s conditions, and the instable intermediates rapidly undergo to consecutive reactions forming novel C-C bonds and subsequently a more recalcitrant structure¹⁹.

1.2.1 “Lignin first” approach

Recently the need to completely valorize the lignocellulosic raw material have led to the so-called “lignin first” approach. In this context, the processes have been optimized in order to avoid/limit the degradation of lignin, promoting either its recovery in the virgin form or its depolymerization toward shorter oligomers (more reactive to further processes) and value-added phenolics compounds (i.e. the lignin “monomers”). One of the most interesting examples is represented by the Reductive Catalytic Fractionation (RCF) i.e. a catalytic promoted fractionation of the biomass in its structural components, performed in the presence of a reductive environment. The process has the advantage to preserve the cellulosic carbohydrates in the solid fraction while lignin is extracted, depolymerized and stabilized by catalytic reduction obtaining a relatively low molecular weight lignin oil containing also phenolic monomers.²⁰

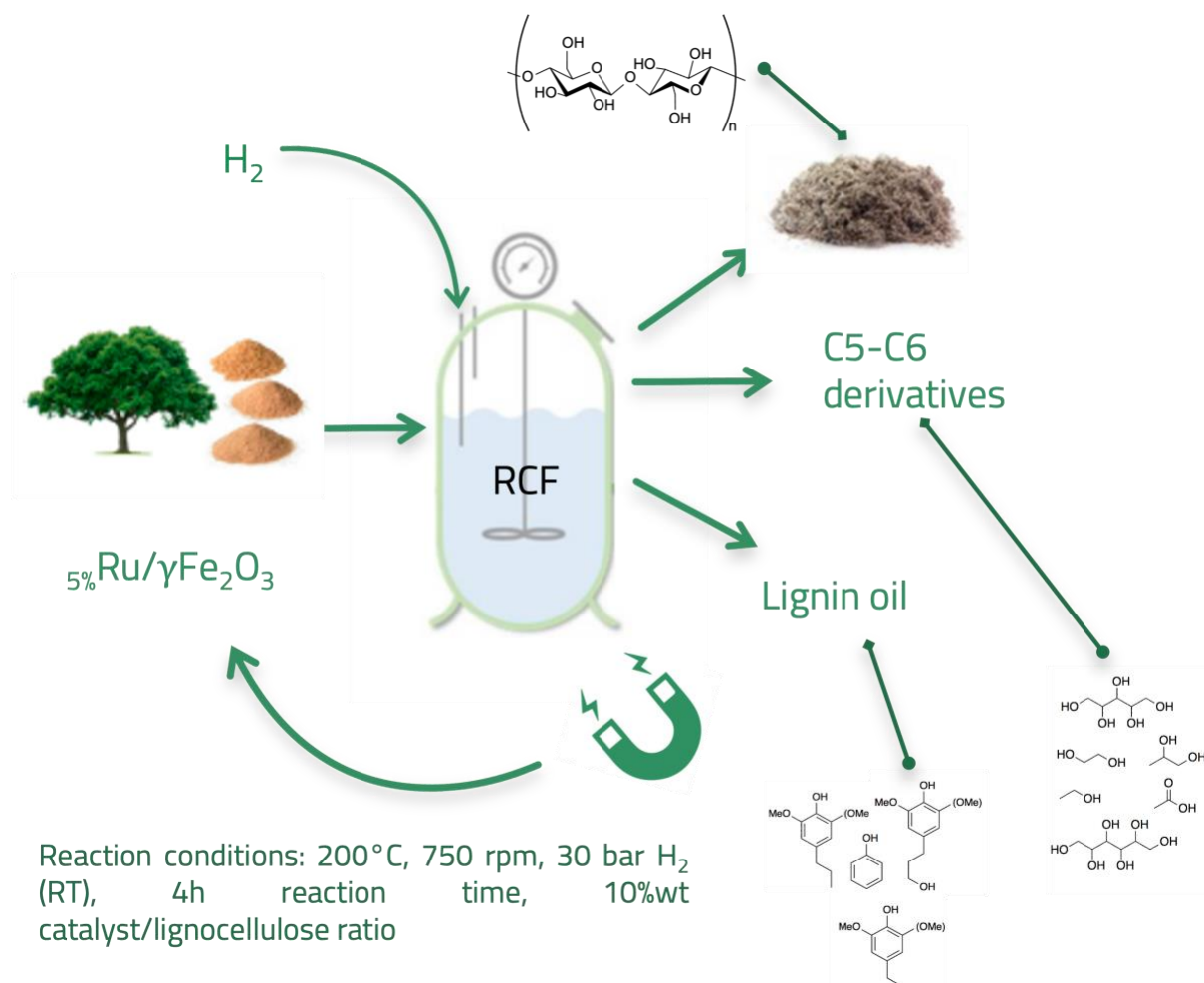


Figure 5 – General scheme of a RCF process.

This process is currently investigated on lab-scale but has the potential to finally valorize every biomass component. Lignin oil can be used as a feedstock to produce pharmaceutical, chemicals and materials, such as resins, adhesives, and coatings²². The cellulosic pulp can be used to produce a variety of products, including paper, cardboard, and bioplastics²¹. Finally hemicellulose fraction could be partially preserved in the pulp or depolymerized and reduced to polyols (mainly xylitol obtained by xylose hydrogenation) and other oxygenated products (depending on the reaction conditions)²³. Interestingly, these polyols and low molecular weight oxygenated compounds can be recovered in water. This diluted aqueous streams, ideally obtainable directly from RCF when binary mixture of water and 1-butanol are used as reaction solvent (Figure 5), can be considered as a low value stream exiting from RCF processes. For this reason, its further valorization, for instance via the consecutive

Aqueous Phase Reforming of the oxygenated compounds (i.e. polyols), is an interesting alternative which may allow to produce green H₂ and develop an overall net zero H₂ consumption process for the valorization of raw lignocellulosic biomasses.

1.2.2 Aqueous Phase Reforming (APR)

Aqueous-phase reforming (APR) is a reaction suitable for biomass derived products to produce hydrogen, alkanes, and other value-added chemicals from biomass-derived resources in liquid water²⁴. Petrochemical processes were designed on hydrophobic, oxygen-free, molecules with high volatility, in order to gain a higher reactivity on those feedstocks those processes were conducted at elevated temperatures and performed in gas phase. The high oxygenated raw material cannot be directly used due to insufficient combustion and low energy content. Therefore, the biorefinery process should limit the amount of oxygen of the bio-based building block chemicals via reductive processes. According to Figure 6, traditional combustion has a low O/C molar ratio (low moisture content), whereas biomass has a high O/C molar ratio (high moisture content), which causes less energy to be generated during combustion. Furthermore, biomass derived compounds are usually more water soluble and richer in functional reactive groups such as hydroxyl and carboxylic acid.²⁵ Consequently, it is possible to design liquid phase processes at lower temperatures, which means oxygenated hydrocarbon reforming is more favorable at low temperatures than alkane reforming, which is more advantageous at high temperatures since alkane reforming requires a greater amount of energy to break the C-C bond in comparison to oxygenated hydrocarbon reforming.²⁶

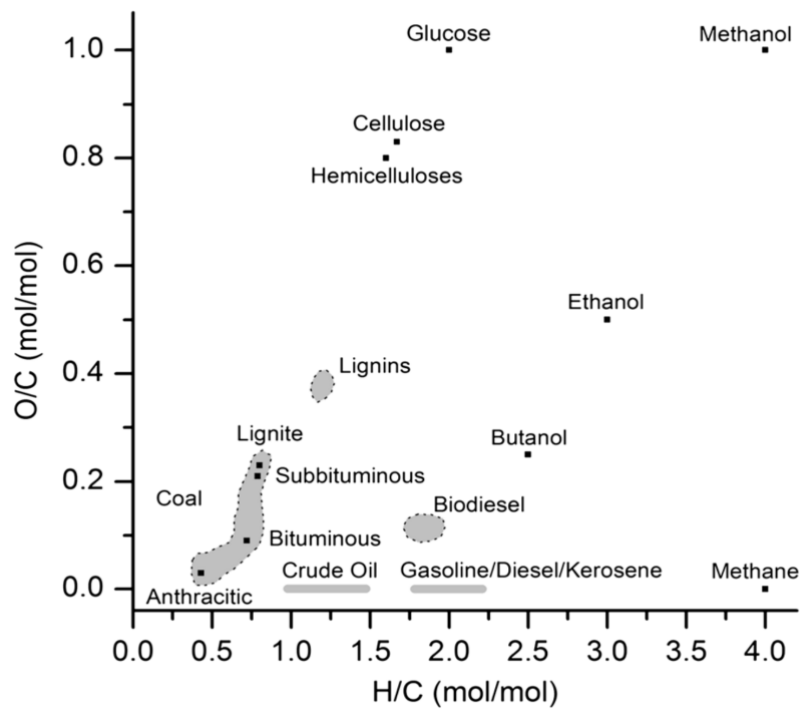


Figure 6 - The O/C and H/C molar ratios of fossil and biomass raw materials and fuels derived from them. Adapted from ref. ²⁶.

For instance, in figure 7 are reported reactions such as hydrolysis, dehydration, isomerization, oxidation, and aldol condensation which are performed at low temperatures, of about 400 K. Hydrogenolysis, hydrogenation, and aqueous phase reforming are performed at relatively higher temperatures (470-500 K) and high pressure (14-50 bar) to maintain water in his liquid state. On the contrary, as anticipated before, steam reforming and other petrochemical processes are performed at harsher conditions .²⁷

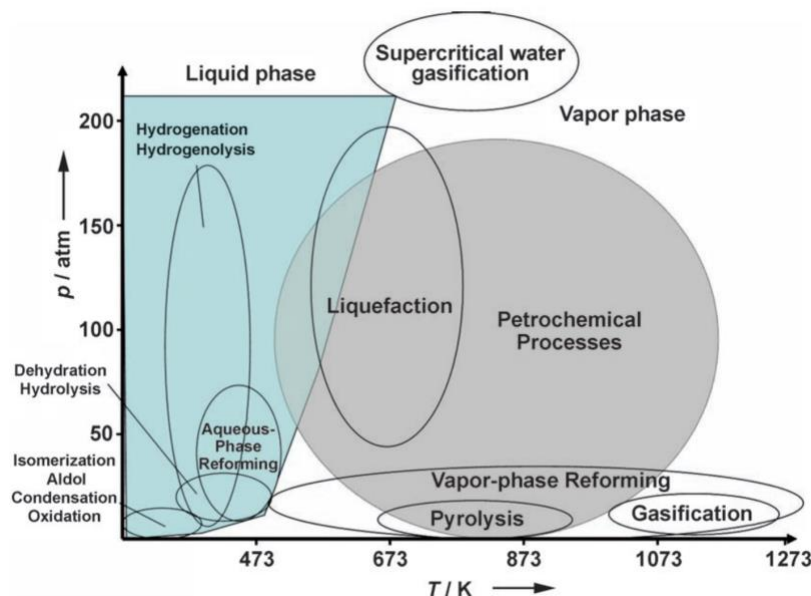


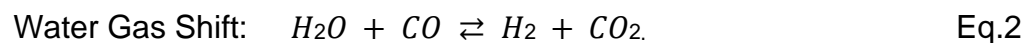
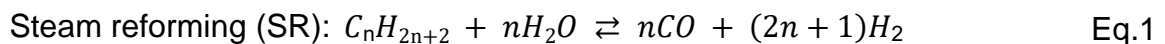
Figure 7 - Diagram of approximate reaction conditions for the catalytic processing of petroleum versus biomass-derived carbohydrates. Adapted from ref.²⁷.

Working at lower reaction temperature is not only energy-saving but lead also to better performance in terms of carbon balance (coke formation from carbonaceous feedstocks is favored at higher temperature such as other undesirable reaction)²⁸. Moreover, working in aqueous phase on biomasses show convenience in terms of avoiding the vaporization of a moisture rich feed. In particular, Aqueous Phase Reforming (APR) could be used to produce H₂ from different biomass derived products such sugars (glucose and fructose), polyols (sorbitol, xylitol, glycerol, and ethylene glycol), ethanol, and other bio-renewable feedstocks (methanol and acetic acid)²⁹ using greener processes compared to the classic steam reforming. By acting on the reaction conditions and the type of catalyst, the process can be driven toward gas phase products to produce H₂ or liquid phase molecules such as acids, alcohols, glycols, and aldehydes for the polymer industry, cosmetics, and chemistry building blocks³⁰. Furthermore, during the APR processes a series of other specific reactions take place, in particular: dehydrogenation of alcohols to hydrogen and aldehydes/ketones, decarbonylation (forming CO) or decarboxylation (forming CO₂), aldol or retro-aldol condensations, Cannizzaro disproportionation and, thanks to the

presence of an excess of water also Water Gas Shift (WGS) reaction which can product H₂ and CO₂ starting from CO finally enhancing the H₂ yield overall.

1.2.3 Thermodynamic and kinetic considerations

The reaction conditions to produce hydrogen from hydrocarbons (alkanes) are dictated by the thermodynamics of 2 reactions:



For sugar derived polyols, compounds with C/O ratio=1, the steam reforming reaction has the stoichiometry:



According to Figure 8, the steam reforming of polyols C1-C5 (such as methanol, ethylene glycol, glycerol, and sorbitol) is thermodynamically favorable at lower temperature than the C1-C6 respective alkanes (such as methane, ethane, propane, and hexane) where SR is thermodynamically favored only at temperatures above 675K (900K for CH₄). The increase of hydrogen and carbon dioxide partial pressures drives the WGS reaction in the reverse direction leading to carbon monoxide coverage of the metal surface and its passivation. On the contrary, working at low temperature with oxygenated compounds favor WGS reaction and makes possible a one-pot catalytic reaction where both WGS and APR are activated. Furthermore, due to the high vapor pressure of the oxygenated products, the reaction of SR takes place in the liquid phase with H₂O as a solvent, thus reduces the need to use additional water for the steam-reforming reaction, and a further increase in the hydrogen production with the WGS reaction³¹. It is also possible that H₂, CO and CO₂ come from liquid phase reactions of dehydrogenation and decarboxylation, but regardless of the reaction path the process is cheaper in terms of energy expenditure and H₂ production in a single reactor²⁶.

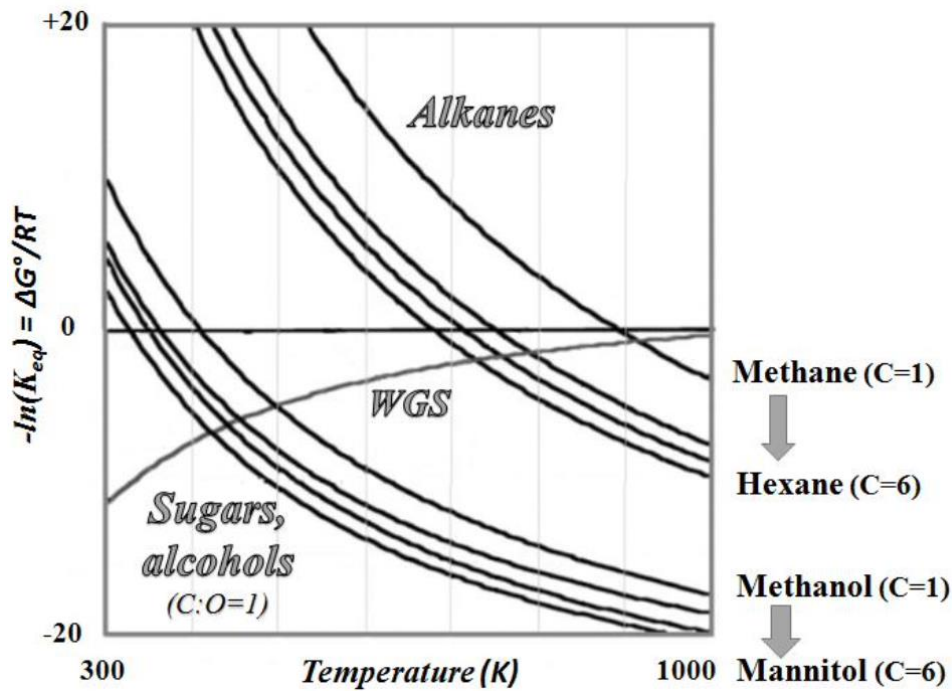
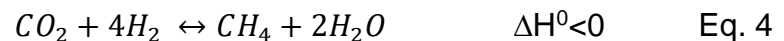


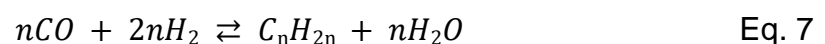
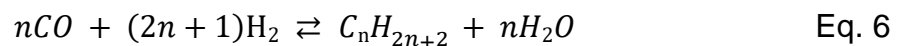
Figure 8 - Gibbs free energy change with temperature for reforming reactions of alkanes and carbohydrates and WGS. Adapted from ref. ²⁶.

If the purpose of the APR reaction is the production of H₂, it must be considered the side reactions that could undergo in the same condition of APR. In the range of temperatures considered for the APR process, the alkane can be produced from subsequent reaction of H₂ and CO/CO₂ via methanation (Eq.4 and Eq.5) and the Fischer-Tropsch reaction (Eq.6 and Eq.7), that are energetically favored instead of reforming, For example, the equilibrium constant at 500 K for the conversion of CO₂ and H₂ to methane (CO₂ + 4H₂ ↔ CH₄ + 2H₂O) is in the order of 10¹⁰ per mole of CO₂.²⁶

Methanation:



Fischer-Tropsch reaction:



Tuning the catalyst features could selectively avoid or favor a certain reaction pathway affecting highly the productibility, selectivity, and yield on desired products. Moreover, the catalyst has the role of promoting the WGS reaction (Eq.2) to remove CO from the metal surface and avoid parallel reactions to oxygenated molecules in water.²⁴ Therefore, for improving APR performance, the undesired reaction like C-O cleavage, methanation, and Fischer-Tropsch synthesis reaction should be avoided.

1.2.4 Catalyst for APR reaction

The choice of catalyst is crucial in a complex mechanism such as APR reaction. The ideal condition to produce hydrogen via APR of oxygenated hydrocarbon should require an efficient catalyst that enhance dehydrogenation and reforming reaction (C-C cleavage followed by WGS) and inhibit the formation of alkane (C-O cleavage followed by hydrogenation).²⁷

As a result, an ideally designed catalyst should favor C-C bond activation over C-O activation as well as WGS over methanation³³, WGS is also fundamental to remove CO from the reaction environment and enhance H₂ yield. Those three parameters for different active phases (metals) are reported in figure 9, the data comes from different studies, the rate of a particular reaction can be compared for the different metals; however, for a specific metal, the absolute rates of the three different reactions cannot be compared relative to each other. In particular:

Sinfelt and Yates studied the activity of different metal active phases over silica evaluating C-C cleavage on ethane hydrogenolysis at 200°C. Grenoble et al.³⁴ studied the relative catalytic activities for water-gas shift over different metals supported on alumina at 300°C with CO and H₂O. Cu shows the highest catalytic activity for WGS but seems only slightly active for C-C bond cleavage, while Pt, Ru and Ni have good activities in both reactions. Vannice³⁵ reported a study on the relative rates of methanation catalyzed by different metals supported on silica (H₂/CO=3 at 275°C).

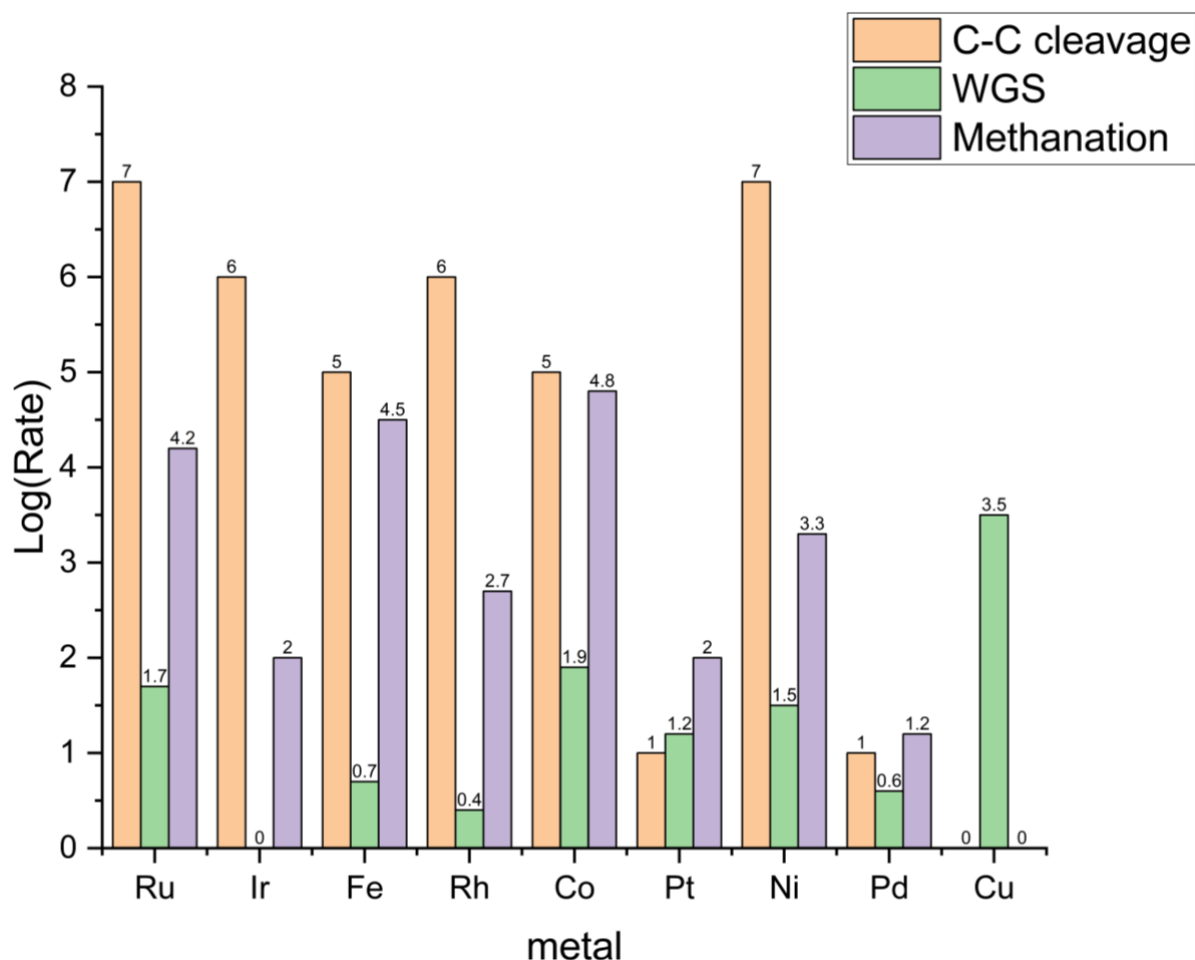


Figure 9 - Catalytic activity of different metal active phases for C-C cleavage, WGS and methanation reaction. Adapted from ref. ²⁶.

Co and Fe have excellent activities in the C-C scission and moderate in the water-gas shift but show tendency to promote methanation too, on the other hand Cu shows the best activity for WGS but doesn't activate C-C cleavage. The Pt and Pd can balance both three components of the reaction, which controls less methanation in comparison with other metals, while at the same time maintaining a high level of C-C cleavage and WGS. It is possible to theorize that Pt and Pd are the best active phases for an efficient catalysis of the APR. ²⁶ Generally speaking, the performance of APR does not depend solely on the choice of metal, but also on other factors such as the type of support, the composition of the support, the loading quantity of metal and the methodology for synthesis, etc., all of which should be taken into account for the calculation.

In literature several factors are reported to control the selectivity of APR process and several are related not only to the active metal phase but also to the characteristics of the support, in particular: ³²

- a) more acidic support can lead to higher selectivity for alkene formation by alcohols/polyols dehydration reactions, the latter could be hydrogenated to alkane. On the opposite, basic or neutral supports can favor hydrogen production. Basicity can polarize water that can facilitate the formation of hydroxide ions, which can act as catalysts for the WGS reaction leading to get higher yields of hydrogen.
- b) Redox couple involves WGS promotion by a redox mechanism.
- c) Supports characterized by meso-porosity, with pore diameters ranging from 2 to 50 nm, are the most investigated due to the enhanced diffusion of reagents avoiding mass transfer limitations.
- d) Oxygen storage and mobility involve WGS promotion.

The acidity or basicity of the reactant solution can influence the reaction path, despite the solvent is water, the aqueous solution could be more or less acidic depending on the makeup of the byproducts and intermediate compounds created in the reactor. Additionally, dissolved gaseous carbon dioxide creates a mildly acidic solution (pH = 4-5) when added to the mixture under high pressure. The acidic solution catalyze dehydration of alcohols to alkenes and other unsaturated compounds which can subsequently undergo hydrogenation reaction to form alkanes. On the other hand, neutral and basic solutions result in a lower alkane selectivity avoiding at the same time H₂ consumption.²⁶

1.2.5 APR feedstocks alternatives

Concerning the feedstock characteristics, model compounds commonly applied in APR include sugars, polyols and alcohols such as glucose, fructose, sucrose, sorbitol, xylitol, glycerol, ethylene glycol, ethanol, methanol, acetic acid, acetaldehyde, acetol, butanol and so on. Interestingly the APR of cellulose is also reported.²⁸ Starting from polyols usually lead to higher hydrogen selectivity compared to the respective sugars. This is due to the different reactivity of the sugars that can readily undergoes to aldol-condensation and cyclisation reaction forming humins.³⁶ Humins could be problematic because they can clog the reactor, decrease the efficiency of the reaction by deposition on the catalyst surface leading to its subsequent deactivation and determine an important loss in terms of carbon balance. Moreover, is possible that these products could be reduced consuming H₂ present in the environment of reaction. Minimize humins formation is crucially important for APR, therefore a fine tuning of both the reaction conditions and catalyst properties is required.

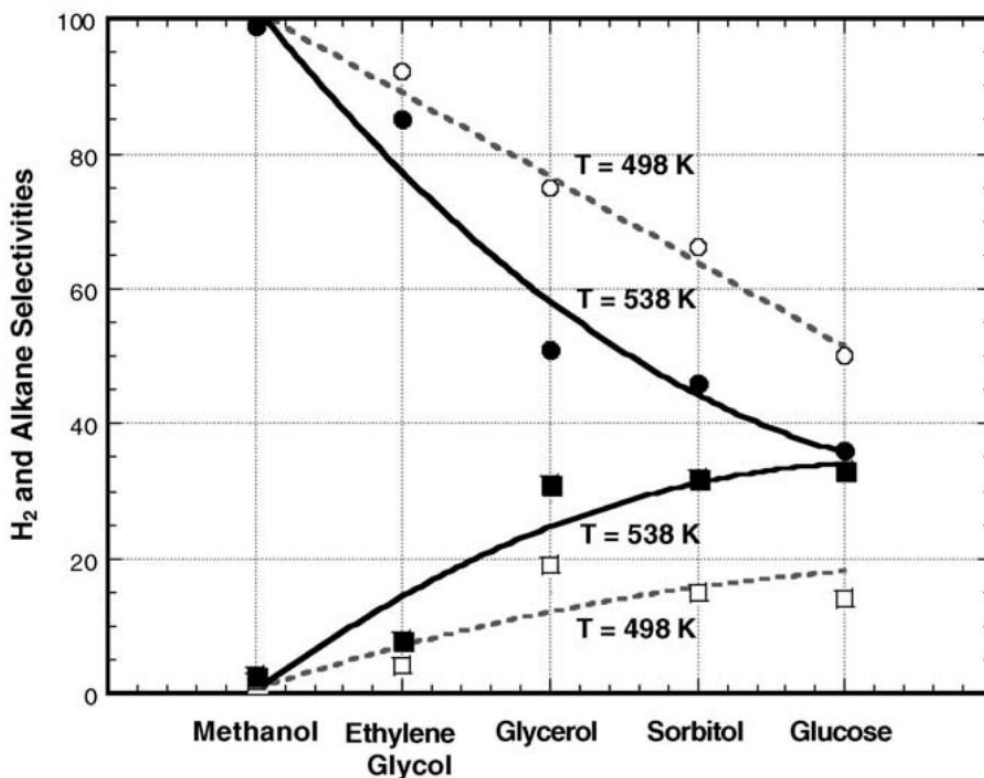


Figure 10 - Selectivity vs. oxygenated hydrocarbon. H₂ selectivity (circles) and alkane selectivity (squares) from aqueous-phase reforming of 1 wt.% oxygenated hydrocarbons over 3 wt.% Pt/Al₂O₃ at 498 K (open symbols and dashed curves) and 538 K (filled symbols and solid curves).²⁶

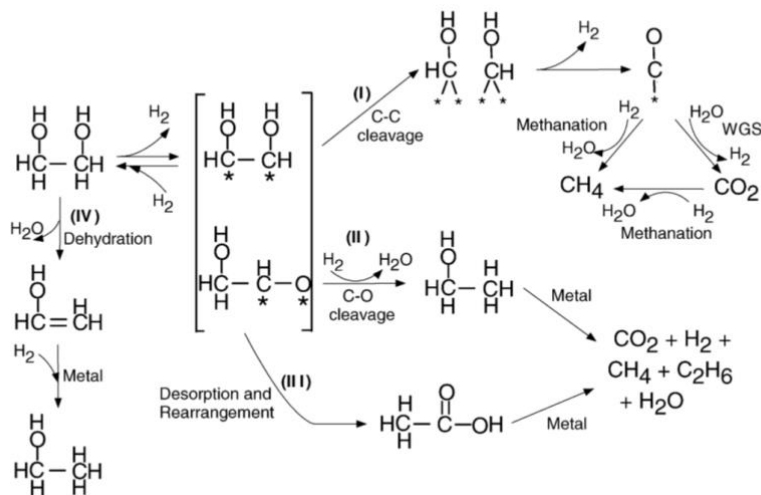
The APR of glucose, sorbitol, glycerol, ethylene glycol and methanol have been widely studied in the literature. Figure 10 indicates that the selectivity of hydrogen and alkane over Pt/Al₂O₃ at 498K and 538K, are highly dependent on the type of feedstock. Usually, the selectivity of hydrogen progressively decreases by increasing the carbon chain length.²⁶ If the chain of carbon becomes longer, the possible reaction pathway will be more complex, increasing the amount of possible intermediates, and the selectivity towards H₂ decrease because of a higher number of possible side reactions. Moreover, working with high feedstock concentration usually leads to higher humin formation while diluting helps raising H₂ selectivity leading to low productivity. This is explained by the fact that humins formation derives from intermolecular reaction, so it is kinetically proportional to feedstock concentration while APR is an intramolecular reaction independent by this parameter³⁷. Another study conducted by Davda and Dumesic²⁶ confirmed that when processing higher concentrations of glucose as a feed,

the hydrogen selectivity decreases. For instance, as the concentration of glucose in the feed increases from 1 to 10 wt.%, the hydrogen selectivity decreases from 50 to 13%, respectively.

1.2.6 Mechanism of APR reaction

APR reaction, as said before, could be applied to different organic feedstocks. In general, gas phase products are H₂, CO (hopefully in low amounts if WGS is efficiently promoted), CO₂, methane, and light alkanes (C₂-C₃), while liquid phase products may be alcohols, diols, aldehydes, acids, and other oxygenated compounds. Depending on the type of catalyst different reactions could be favored, for instance, C-C cleavage, C-O cleavage, dehydrogenation, hydrogenation, hydrogenolysis, hydration and dehydrogenation, are typical reactivities involved in these processes. Furthermore, the presence of highly reactive compounds such as aldehydes and alcohols may generate tautomeric equilibria, aldol condensation reactions, isomerization, polymerization and cyclization as well.³⁸

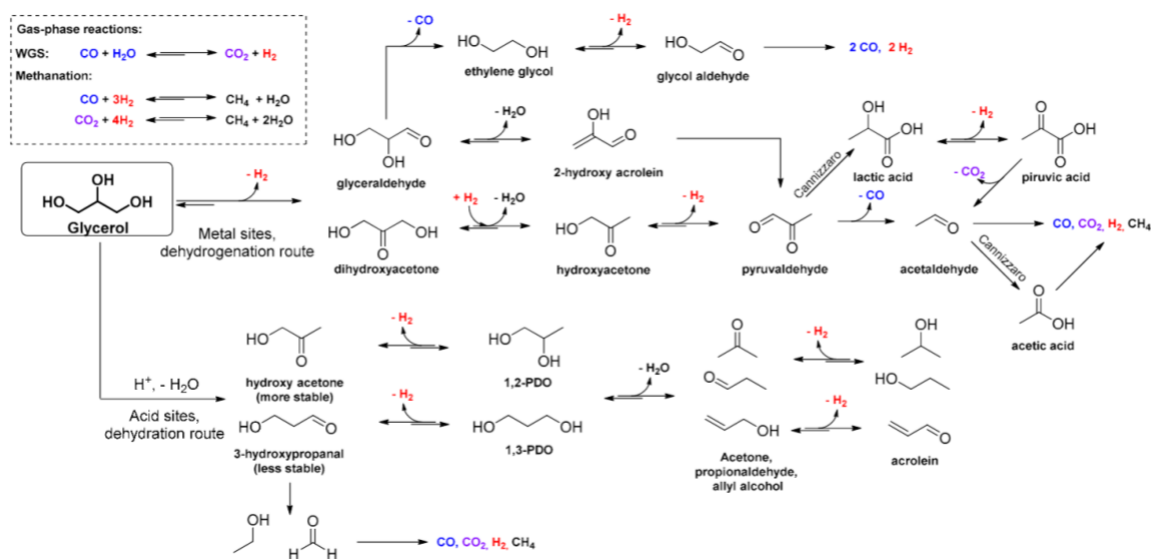
A reaction scheme of the APR of ethylene glycol (EG) has been hypothesized using a Pt-based catalyst (Scheme 1). After a first dehydrogenation step, the type of absorption on the metal surface determines the consecutive reactivity, in particular the C-Pt-C bond (more stable than C-Pt-O), lead to a C-C cleavage pathway (I) towards C1 activated species absorbed on the metal surface. After the desorption of H₂, CO is deposited on the surface of the catalyst where, eventually, WGS or methanation occur. On the other hand, absorption of C-O bond is also possible, this bond can undergo HDO towards ethanol through C-O cleavage and stabilization via hydrogenation (II) or a desorption and rearrangement towards acetic acid (III). Alternatively, acid catalyzed (support acid sites/organic acids in solution) dehydration could happen as first reaction on EG towards acetaldehyde (or ethanol through further reduction) (IV).



Scheme 1 - reaction paths in the aqueous phase reforming of ethylene glycol. ²⁶

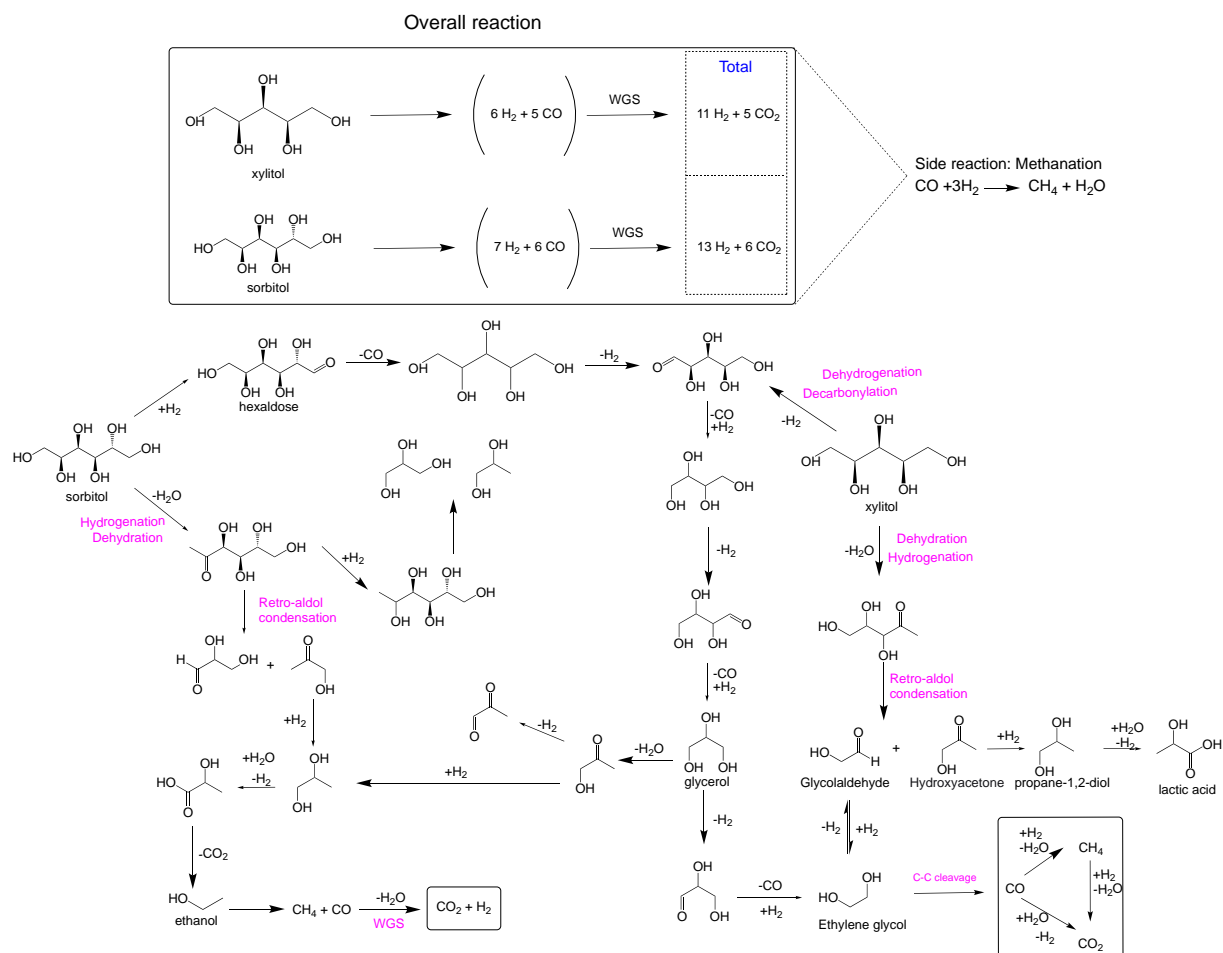
As remarked in other sections of this work, it is clear that higher selectivity of hydrogen are linked with high activity on C-C cleavage and low activity on C-O cleavage.

By adding a C atom to the feedstock chain (Glycerol instead of EG), the reaction pathway gets dramatically more complicated. Intuitively, glycerol has more intermediates which can undergo further reactions, however the families of possible reactions are similar, include reversible dehydrogenation process, C-O and C-C bond cleavage on metal site, and dehydration on acid site.



Scheme 2 - Possible reaction pathways occurring in glycerol aqueous phase reforming (APR).

Adapted from ref. ³⁹

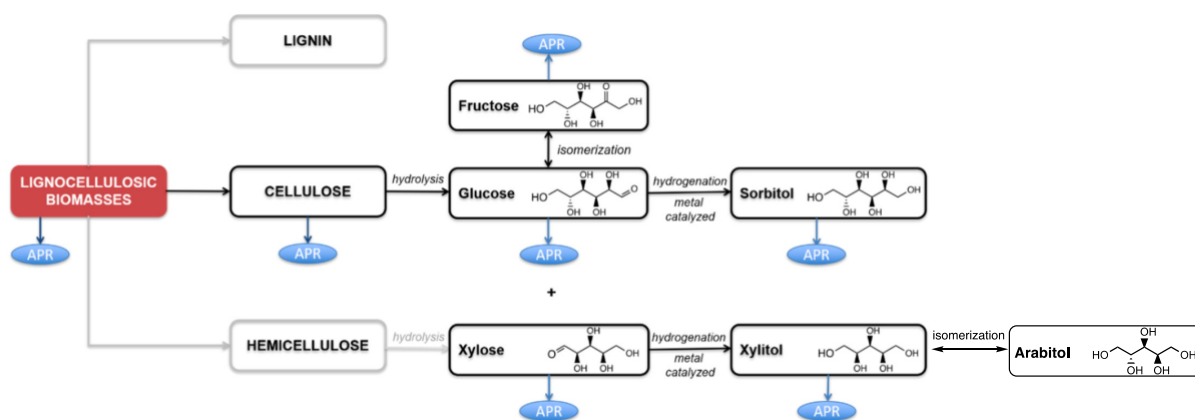


Scheme 3 - Possible reaction pathways occurring in aqueous phase reforming (APR) of polyols, namely sorbitol (C6) and xylitol (C5). Adapted from ref.⁴⁰

As deduced from glycerol, when C5-C6 chains are involved, the mechanism become extremely complicated (see scheme 3). The key step of APR on C5 and C6 seems to be Retro-aldol C-C cleavage which reduce long carbon chain to C3 or C2. Therefore, the function of catalyst is vital for retro-aldol condensation and further reforming reactions. In this case, the retro-aldol condensation seems to happen at the very beginning of the reaction when there are more oxygen atoms on the feed molecule. According to literature, this step can happen at acid, basic or even neutral conditions.⁴¹

Although xylitol is the second most abundant polyol produced by the lignocellulosic processing industry as a result of xylose hydrogenation, its significance is largely overlooked; however, studies on the formation of hydrocarbons from sugar alcohols, including xylitol, are of critical importance. The APR should investigate and compare

the performance of xylitol, one of the most abundant building blocks of natural polymers.



Scheme 4 - Lignocellulosic biomass average composition and valorization processes, namely hydrolysis, hydrogenation, and Aqueous Phase Reforming (APR), Adapted from ref. ⁴⁰.

2 THESIS SCOPE

An increasing number of industrial chemists are interested in aqueous phase reforming reactions for their potential to upgrade waste aqueous solutions containing polyols or sugars that otherwise would be considered dead ends. APR reactions also possess low energy requirements along with intrinsic safety and low CO emissions. It is a catalytic process that produces hydrogen, alkanes, or chemicals depending on the conditions of the reaction and the catalyst.

Xylitol is the second most abundant polyol produced by the lignocellulosic processing industry and can be used in this process to produce substantial quantities of H₂ or acids and glycols in liquid form. The productivity of the process is heavily dependent on the catalyst, most of the studies in the literature have been conducted with scattered experiments over different metals, in particular platinum, and less with other supports. This work seeks to provide an analysis, as complete as possible, of how parameters and catalyst characteristics effect xylitol APR, correlating catalyst characterization with reactivity data.

3 EXPERIMENTAL PART:

3.1 Specific reactor

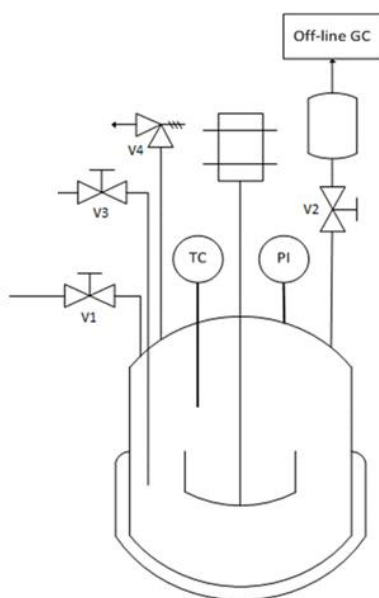


Figure 11 – Schematic of the autoclave reactor used for the APR of xylitol

The reactor used to carry out the catalytic tests is a stainless-steel Parr autoclave with an internal glass container. The steel reactor body and cap are joined with a Teflon gasket and held closed by screw clamps.

In the head of the reactor are allocated a pressure gauge, an impeller for stirring, a rupture disk having the function of a safety device (V4), two needle valves (one of which with a Swagelok type fitting), an electronic pressure gauge, a thermocouple, and a gas sampling system. The valve with Swagelok type fitting (V3) is connected to a steel pipe drawing into the reaction mixture.

The pressure gauge and thermocouple have electrical connections to an external controller, which is also connected to the motor needed to move the impeller. Heating is provided by a heating mantle, into which the lower part of the reactor is completely inserted. The shell is connected to the electronic controller which regulates the heating

based on the measurement of the temperature inside the reactor provided by the thermocouple, the controller also allows to read the internal temperature, the internal pressure relative to the external one with great precision and to adjust the speed of agitation.

The gas sampling system consists of an expansion barrel equipped with a septum for sampling; the connection between the head and the gas sampling system is equipped with a needle valve (V2) which serves to prevent the reaction mixture from rising during the reaction itself. The sampling septum is mounted on a tee connected to the barrel; to close the system, a cap nut is screwed onto the other free end of the T-piece.

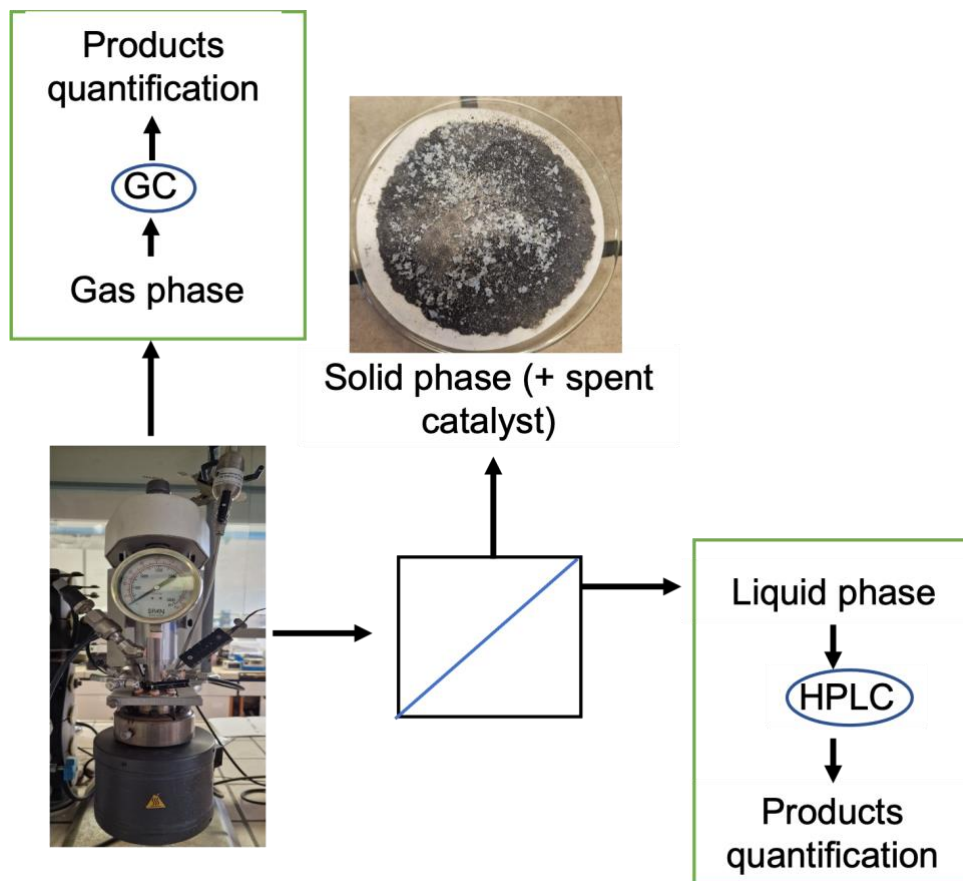
3.1.1 Reaction procedure

The reaction mixture is prepared in a glass vessel by inserting: 50mL of water and 1.50g of xylitol (0.00987 mol) or an equivalent molar amount of glycerol, lactic acid or other intermediates depending on the test to be performed. The catalyst, typically 0.45g, is added to the solution and the vessel is inserted into the reactor. The reactor is sealed and flushed for about 10 minutes with 5.2 bar of nitrogen. The charged reactor is then housed in the heating mantle, connected to the electronic pressure, temperature and stirring controller and started. Before heating, make the inside pressure of nitrogen is equal atmospheric pressure (1 bar). The heating time taken by the shell to reach the target T of the reaction is approximately one hour, once the isothermal conditions are reached, the reaction is carried out for the desired time.

After the reaction time has elapsed, the heating is stopped, the heating mantle removed, and the reactor immersed in an ice bath. Once ambient temperature has been reached, the needle valve (V2) is open to allow the gas to reach the pierceable rubber septum and be withdrawn to analyze the gaseous phase in the GC. Finally, the reactor is dismantled and unloaded. The reaction mixture is separated from the catalyst by vacuum filtration on a Buchner type filter with filter paper. The catalyst is dried in an

oven at 80°C and stored for possible analyses, while the reaction mixture, after having measured its volume and pH, is stored in a refrigerator at 4°C for subsequent HPLC analyzes of the products.

A simplified reaction scheme of the different stream obtained after reaction is reported in scheme 5.



Scheme 5 - Analytical approach for the identification of reaction products and intermediates in APR of xylitol.

3.2 Catalysts synthetic procedures

3.2.1 Synthesis of magnesium oxide (MgO)

Magnesium oxide is prepared by precipitation at constant pH (10.5 ± 0.2) and temperature ($60 \pm 2^\circ\text{C}$) by slowly adding 2 M of $\text{Mg}(\text{NO}_3)_2 \cdot 6\text{H}_2\text{O}$ solution into a solution

of Na_2CO_3 [1M]. Before adding the Mg containing solution, the pH was brought to the desired value by adding HNO_3 . The solution containing the cations was then added slowly drop by drop, keeping the carbonate solution under vigorous stirring and counterbalancing the pH variations by adding 4M NaOH. Once the addition of the cationic solution to the anionic one was completed, the precipitate was kept under stirring at pH 10.5 and at a temperature of 60°C for about one hour. The solid was then recovered by filtration and washed with distilled water to reduce the concentration of Na^+ and remove the nitrates. The solid thus obtained was dried in an oven at 105°C for one night and calcined at 400°C for 3 hours following a temperature ramp of $10^\circ\text{C}/\text{min}$.

3.2.2 Synthesis of Magnesium/Aluminum mixed oxide (MgAlOx)

Synthesis of mixed oxides are obtained through the calcination of an hydrotalcite precursor.

The hydrotalcite precursors $[(\text{M}^{2+})_{1-x}(\text{M}^{3+})_x (\text{OH})_2]^{x+} [(\text{An}^-)_{x/n} \text{mH}_2\text{O}]$ were prepared by co-precipitation at constant pH (10.5 ± 0.2) and temperature ($60 \pm 2^\circ\text{C}$) by adding a solution of cations [4M] (Mg and Al in a ratio of 75:25) added as nitrate salts to a solution of Na_2CO_3 [1M] ensuring an excess of carbonates equal to 6 times of the stoichiometric amount of charged 3+ ions (i.e. aluminum). Before adding the cations, the pH was brought to the desired value by adding HNO_3 . The solution containing the cations was then added slowly drop by drop, keeping the carbonate solution under vigorous stirring and counterbalancing the pH variations by adding 4M NaOH. Once the addition of the cationic solution to the anionic one was completed, the precipitate was kept under stirring at pH 10.5 and at a temperature of 60°C for about one hour, then filtered and washed with distilled water to reduce the concentration of Na^+ and

remove the nitrates. The solid thus obtained was dried in an oven at 105°C for one night and calcined at 400°C for 3 hours following a temperature ramp of 10°C/min.

3.2.3 Synthesis of Pt- supported catalysts

The Pt catalysts investigated in the present work were obtained via supportation of the metal over different metal oxides, such as Fe₃O₄, a commercial γ -Al₂O₃, and MgAl mixed oxides (MgAlOx) in particular via incipient wetness impregnation (IWI). As an example, the mud point of the MgAlOx with an atomic ratio of Mg/Al equal to 3:1) was firstly evaluated adding drop-by-drop a precise volume of distilled water. In this way an apparent pore volume of the material was obtained (0.8443 cm³/g). Then the desired amount of Pt precursor (i.e. tetra ammine platinum (II) nitrate, Pt(NH₃)₄(NO₃)₂) was dissolved in two times the volume of the pore of the weighted mass of support. The Pt precursor needed was calculated to allow us to obtain a 5 wt.% of Pt element respect in the final catalyst. The impregnation was performed two times, with an intermediate heat treatment at 60°C for 1 hour between the two impregnations. The impregnated material was then dried in an oven overnight at 105°C and calcinated at 400°C for 3 hours, finally the catalyst was reduced at 250°C for 2 h in a 10% H₂ in N₂ flow using a temperature ramp of 5°C/min.

3.3 Gas phase analysis

The compounds of interest were analyzed and quantified using a gas-chromatograph Hewlett Packard 5890 Series II GC instrument equipped with TCD detector and two capillary columns with Argon as carrier:

1. Agilent CP-Molsieve 5A capillary column (25m x 530 μ m x 50 μ m), connected to a thermal conductivity detector (TCD) detector and used to elute and quantify H₂, O₂ and N₂.

2. Agilent CP-SilicaPLOT capillary column (30m x 530 μm x 6 μm), connected to the TCD and used to elute and quantify CO, CO₂, CH₄, ethylene, propylene and propane.

The gas sampling is extracted from a needle valve (V2) of autoclave by 1ml of syringe. Before injecting in the GC, the syringe must discharge the air from the needle and repeat three times. Measure 0.6ml of gas mixture to GC as quick as possible. The quantification of gas phase products was achieved by calibration of the single products H₂, CO, CO₂, CH₄ and ethylene.

It was decided to use only one analysis to quantify ethane and propane, which have high retention times, as they are always minority or absent products, as well as to save time in the analyses.

The three GC analyzes of the gas mixture samples are performed according to the following column thermostatisation method, for a duration of 31.33 min:

8 min isotherm at 40°C, 12°C/min heating to 170°C, 4 min isotherm at 170°C, 12°C/min heating to 200°C, 6 min isotherm at 200 °C.

3.4 Liquid phase analysis

Quantification of liquid products was performed by HPLC analysis, to eliminate any solid and dust particles each sample is filtered with a PPE syringe filter with a pore size of 0.45 μm .

The chromatographic column chosen for the separation of the compounds obtained in the liquid phase is a Phenomenex Rezex ROA, 300x7.8 mm, 8 μm particles. This column is packed with a stationary phase consisting of a sulfonated styrene-divinylbenzene resin. The mobile phase used for the analyzes is a solution of H₂SO₄ 0.0025 mol/L in ultrapure water. The HPLC chromatograph used is Agilent Infinity 1260 with two detectors in series: a Diode Array Detector (used for UV absorbers) and Refraction Index detector. The conditions used include a flow of 0.500 mL/min and the

execution of two different analyzes for each sample, the column separation is performed at 80°C then the stream pass through the DAD detector and RID detector at 40°C, the analysis is 120 min long and the products are quantified by calibration using commercial standards.

3.5 Calculations

The quantification of both gas and liquid phase products were performed through calibration curves which linked the instrument signal related to each compound to its concentration (for liquid phase) or the mole number (for gas phase).

Gas products yields (Y) were calculated as a mean of 3 GC injections over the total amount of reagent initially charged in the reactor. For each product a stoichiometric factor (SF) was calculated considering the conversion of a reagent A towards a selected gas product B:

$$(1) Y_B = \frac{n_{B \text{ inj}}}{n_{\text{tot inj}}} \times \frac{P_{\text{autoclave}} \times V_{\text{autoclave}}}{0,08314 \times T(K)} \times \frac{100}{n_{A_i} \times SF}$$

SF= 6 for H₂; 5 for CO, CO₂, CH₄; 2,5 for C₂H₆, C₂H₄

Liquid products yields (Y) were calculated over the total amount of reagent as well, considering the complex scheme of reaction, for each product a stoichiometric factor based on C atoms (SFC) was used. This factor is calculated from the ratio of C atoms contained in the selected product B and the C atoms contained in the initially charged reagent A

$$(2) Y_B = \frac{n_{C_B}}{n_{C_{A_i}}} = \frac{M_B \times V_{\text{liquid phase}} \times SFC \times 100}{n_{A_i}}$$

SFC= 1 for C₅ products, 4/5 for C₄ products, 3/5 for C₃ products, 2/5 for C₂ products and 1/5 for C₁ products

Selectivity (S) and conversion (X) are calculated similarly, considering the C content, as well as product distribution (XD_B).

$$(3)S_B = \frac{nC_B}{nC_{Ai} - nC_{Af}} \times 100$$

$$(4)X_A = \frac{nC_{Ai} - nC_{Af}}{nC_{Ai}} \times 100$$

$$(5)XD_B = \frac{nC_B}{\Sigma nC_{product}} \times 100$$

From the quantification of C atoms reacted towards products, or unreacted, it is possible to formulate a Carbon Balance (CB) to have an indication of the quantity of undetected C-containing products, for example lost by the production of humins or other heavy products. Thus, can give an indication of the atom efficiency and, subsequently, of the sustainability of the whole process.

$$(5)CB = \frac{nC_{Af} + \Sigma nC_{products}}{nC_{Ai}} \times 100$$

Another parameter used in the data discussion was H₂ productivity (respect to catalyst amount)

$$(6)P_{H_2} = \frac{n_{H_2}}{g_{CAT}}$$

Where:

- A =reagent.
- n_B =moles of product.
- nC_B = carbon moles of product.
- nC_{Ai} = initial carbon moles of reagent.
- n_{H₂} = moles of hydrogen.
- B = product.
- n_A =moles of reagent.
- nC_A = carbon moles of reagent.
- nC_{Af} = final carbon moles of reagent.
- g_{CAT}= mass of catalyst.

3.6 Catalyst Characterization

The catalysts were characterized by manifold techniques in order to investigate the physicochemical properties and to establish correlations with catalytic data.

3.6.1 X-ray diffraction analysis (XRD)

Hydrotalcite precursors, mixed oxides, activated and spent catalysts were characterized by X-Ray Diffraction (XRD) analysis. The analyzes were carried out at room temperature using a Philips X'Pert X'Celerator diffractometer, using Cu radiation (specifically the emission wavelength $K\alpha$, 1.5718 nm). The acquisitions were made with increments of $0.1^\circ/s$ in the interval between 5 and $80^\circ 2\theta$.

In Figure 12 the operation of an X-ray diffractometer is schematized.

The analysis is carried out by making a collimated beam of X-rays affect the sample, which is diffracted only in particular directions of space, depending on the crystalline phases present, following Bragg's law:

$$n\lambda = 2d\sin\theta$$

With:

- n = order of diffraction
- λ = wavelength of the beam
- θ = angle of diffraction
- d = lattice distance between two adjacent atomic planes

The intensity of the diffracted beam is reported as a function of the angle of diffraction. Each diffraction reflection is connected by Bragg's law to a certain interplanar distance d ; for this reason, the analysis of these distances, characteristics for each crystalline cell, it is possible to identify the phase present by comparing the diffractogram with those recorded by the JCPDS standards.

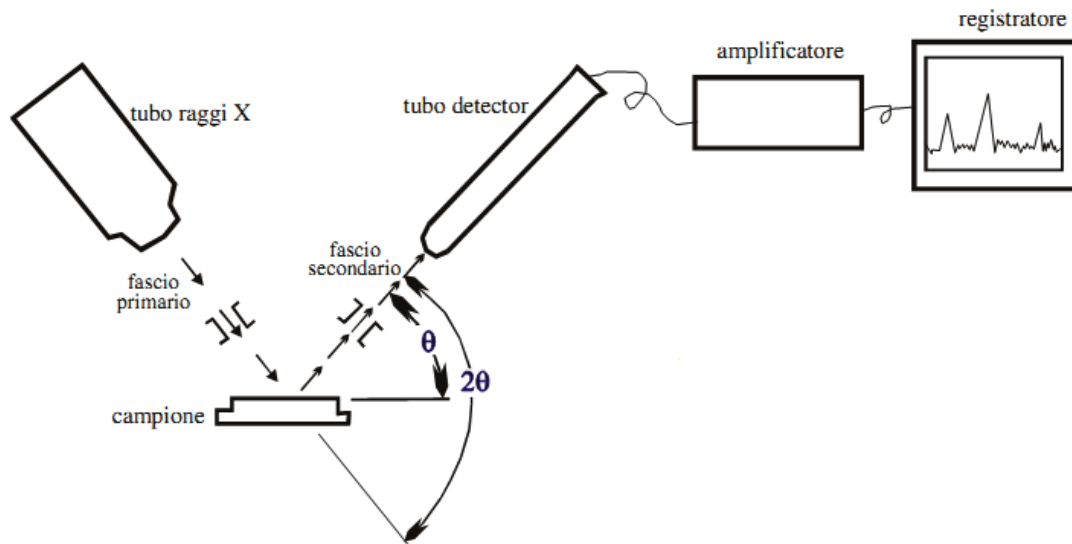


Figure 12 - schematic representation of an X-ray diffractometer for dust analysis

In addition to the determination of the crystal structure via Bragg's law, the XRD spectrum is characteristic of each crystal structure and therefore represents a fingerprint of the compounds. For example, in the spectra of hydrotalcites or HTlc there are 3 typical peaks with height ratios 6:3:2 and variable distance i . Through Sherrer's law it is also possible to calculate the particle size through the formula:

$$d = \frac{k \times \lambda}{b \times \cos\theta}$$

Where: d = size of the crystallites; λ =wavelength of the X-ray (therefore $\lambda_{Cu-K\alpha}$) ; k =shape factor, typically 0.9 but depends on the shape of the crystallite; $b = \sqrt{(2B^2 - \beta^2)}$ (B = mid-height reflex width and β = instrumental stretch); θ = Bragg angle.

3.6.2 Brunauer-Emmett-Teller analysis (BET)

The BET surface area of catalysts was determined by N₂ physisorption at the temperature of liquid N₂ using a Sorptly 1750 Fison instrument. A sample of 0.2 g was initially outgassed at 150 °C before N₂ absorption. The value of the surface area obtained was then divided by the mass of the sample to obtain SSA.

3.6.3 Description of CO₂-TPD, NH₃-TPD and TPR

All experiments were carried out on 0.2 g of sample using a Micromeritics Autochem II 2920 instrument equipped with a TCD detector.

CO₂-TPD

The sample was heated up from room temperature to calcination temperature at a rate of 10 °C/min in a flow of pure He (30 mL/min) to clean surface of the material from physisorbed and chemisorbed molecules. The final temperature was kept for 60 min. After cooling down to 40 °C in a pure He flow (30 mL/min), the chemisorption of CO₂ was carried out by flowing a 10% CO₂/He mixture (30 mL/min) for 60 minutes. After the chemisorption, the sample was flown with pure He (30 mL/min) for 60 min to remove the weakly physisorbed probe molecules. Finally, the temperature programmed desorption was carried out by heating the sample from 40 °C up to calcination temperature at a rate of 10 °C/min in a flow of pure He (30 mL/min); the final temperature was kept for 60 minutes. In order to remove any traces of water before the TCD detector, the effluents from the samples were flown through an empty trap immersed in solid ethylene glycol cooled down to around -60 °C with liquid N₂.

NH₃-TPD

The sample was heated up from room temperature to calcination temperature at a rate of 10 °C/min in a flow of pure He (30 mL/min) to clean surface of the material from

physisorbed and chemisorbed molecules. The final temperature was kept for 60 min. After cooling down to 100 °C in a pure He flow (30 mL/min), the chemisorption of NH₃ was carried out by flowing a 10% NH₃/He mixture (30 mL/min) for 20 minutes. After the chemisorption, the sample was flown with pure He (30 mL/min) for 60 min to remove the weakly physisorbed probe molecules. Finally, the temperature programmed desorption was carried out by heating the sample from 100 °C up to calcination temperature at a rate of 10 °C/min in a flow of pure He (30 mL/min); the final temperature was kept for 60 minutes. In order to remove any traces of water before the TCD detector, the effluents from the samples were flown through trap filled with soda lime and kept at room temperature.

TPR

The sample was heated up from room temperature to calcination temperature at a rate of 10 °C/min to clean surface of the material from physisorbed and chemisorbed molecules by flowing a 5 % O₂/He mixture (30 mL/min). The final temperature was kept for 60 min. After cooling down to 50 °C in a pure He flow (30 mL/min), the sample was flown with a 5% H₂/Ar mixture (50 mL/min) for 30 minutes to allow stabilization of the TCD detector signal. Then, the sample was heated up from 50 °C to calcination temperature at a rate of 10 °C/min and the final temperature was kept for 60 min. In order to remove any traces of water before the TCD detector, the effluents from the samples were flown through trap filled with a 3 Å molecular sieve and kept at room temperature.

3.6.4 Microwave plasma-atomic emission spectroscopy (MP-AES)

Eventual metal leaching from the catalyst to the aqueous solutions was measured by microwave plasma-atomic emission spectroscopy (MP-AES) analyses using an Agilent Technologies 4210 MP-AES instrument. Post reaction solutions were filtered with a 0.2-micron TEFLON syringe filter to completely and effectively remove the heterogeneous catalyst from the solution. Then the obtained solution was diluted in distilled H₂O to fall within the range of the calibration curve (0-300 ppm). The emissions at 358.119nm, 385.991nm and 371.993nm for iron, 285.213nm, 383.829nm and 518.36nm for magnesium, 308.215nm, 394.401nm and 396.152nm for aluminum, 270.240 nm, 304.263 nm and 306.471 nm for platinum were evaluated. The mol% of leached elements were calculated taking into account the actual number of elements present over the catalysts (solution) evaluated by analogous MP-AES analyses performed via the complete acid mineralization of a precise amount of catalyst and proper dilution in water.

3.6.5 Thermal gravimetric analysis (TGA)

TGA analyses were performed with a SDTQ 600 instrument, typically on 15 milligrams of sample charged into an alumina pan. Depending on the kind of information needed, three different thermal treatments were employed. To investigate the transformations occurring during catalyst precursors calcination, the samples were heated up to 650°C with heating rate of 5°C/min in 100 mL/min of air and the final temperature was kept for 1 hour. To measure the mass of carbon deposited on catalyst surface after reaction, the samples were heated up to 650°C with heating rate of 5 °C/min in 100 mL/min of N₂; the final temperature was kept for 1 hour to desorb volatiles and volatile

carbonaceous matter. Then, the gaseous flow was switched from N₂ to air for 1 hour in order to burn all the residual carbon on catalyst surface.

3.7 Chemicals

Chemicals for catalyst preparation: Na₂CO₃ (98%, Alfa Aesar), NaOH pellets (98%, Alfa Aesar), double distilled water (MilliQ, Millipore).

Metal precursor: Mg(NO₃)₂*6H₂O (98%, Alfa-Aesar), Al(NO₃)₃*9H₂O (98%, Alfa-Aesar), Fe(NO₃)₃*9H₂O (98%, Sigma-Aldrich), Ru(NO)(NO₃)_x(OH)_y x+y=3 (1.5%v/w solution, Alfa-Aesar), iron (II,III) oxide (97% trace metals, Sigma-Aldrich), Tetraammineplatinum(II) nitrate (99.99%, Alfa Aesar, Premion®) Pt(NH₃)₄(NO₃)₂

Chemicals for HPLC calibration and APR reaction: Lactic acid (90%, Fluka), pyruvaldehyde (40%, Sigma-Aldrich), hydroxyacetone (95%, Alfa Aesar), pyruvic acid (98%, Alfa Aesar), sorbitol (99%, Sigma-Aldrich), xylitol (99%, Alfa Aesar), formic acid (98%, Fluka), ethylene glycol (99.5%, Fluka), propylene glycol (98% Sigma- Aldrich), 1-propanol (98%, Sigma-Aldrich), ethanol (99.8%, Sigma- Aldrich), acetone (99.8%, Sigma-Aldrich), methanol (99.8%, Sigma-Aldrich), glycerol (99.5% Alfa Aesar), glyceraldehyde (90%, Sigma-Aldrich).

4 RESULTS AND DISCUSSION:

4.1 Magnetic catalysts: 5%wt Pt/ γ -Fe₂O₃

Recently, the Catalysis for Renewable and Innovative Process “Care in Process” group of the Industrial Chemistry Department “Toso Montanari” of the University of Bologna in which I have performed my internship have filed a patent in which an innovative 5%wt Ru/ γ -Fe₂O₃ is used to promote the RCF process of lignocellulosic biomass⁴². Following a similar strategy, we decided to start our investigation from a similar,

magnetic, material a 5%wt Pt/ γ -Fe₂O₃ investigating the effect of the reaction temperature between 200 to 250°C keeping the reaction time at 1h. Interestingly, the magnetic support maghemite, has been chosen also for the advantage of use a magnetic separation of the catalyst at the end of reaction, in this way, future tests on solid cellulose can be conducted greatly limiting the issues of having to separate the solid catalyst from the solid, fibrous, cellulose residue. Results are reported in Table 1 and, while is clear from conversion and carbon balance (CB) that at 250°C an important part of the carbon is lost in heavy products, lower temperature didn't allow us to detect a proper H₂ yield. For initial screening we then decided to keep these reaction conditions to evaluate the activity of different catalysts.

	200 °C	225 °C	250 °C
H ₂ yield (%)	0.50	1.77	4.67
Carbon balance (%)	44.27	37.17	37.35
Conversion (%)	58.19	71.82	95.71

Table 1 – Effect of different reaction temperature in the APR of xylitol with 5 wt.% Pt/ γ -Fe₂O₃.

Condition: 3% wt. of Xylitol in water, 0.45g catalyst, 300rpm, 1h.

In order to test the effect of different metal active phases, comparison between 5 wt.% Pt/ γ -Fe₂O₃ and 5 wt.% Ru/ γ -Fe₂O₃ catalyst were made. It can be seen from Table 2 that highest hydrogen yield was shown by Pt active phase. In terms of CB as well, Pt achieve higher performances, one possible explanation is a major tendency of Ru to promote the formation of high molecular weight byproducts or some alkene gases that cannot be detected by HPLC and GC.

	Pt/ γ -Fe ₂ O ₃	Ru/ γ -Fe ₂ O ₃
H ₂ yield (%)	4.67	2.58
Carbon balance (%)	37.35	33.43
Conversion (%)	95.71	79.76
Selectivity of isomer (%)	44.43	53.52

Table 2- Comparison of the catalytic activity of different metal, namely Pt and Ru (5 wt.%) over γ -Fe₂O₃. Condition: 3% wt. of Xylitol in water, 0.45g catalyst, 300rpm 250°C, 1h.

More in depth analysis on liquid products are not reported in this work but the main product of the reaction seems to be a xylitol isomer, arabitol, as suggested by a crosschecking of HPLC and ESI-MS analysis. This mechanism doesn't involve any C-C cleavage nor positive hydrogen production, both fundamental for the APR process. As proposed by Xia and Jin, in liquid phase, xylitol is dehydrogenated to xylose, xylulose and 3-pentulose in α , β and γ -position, respectively. These pentoses are hydrogenated towards xylitol, arabitol and adonitol⁴³. Those kind of isomer can continuous form smaller intermediate, such as glycerol, 1,2-PDO and EG. In this case, the isomer selectivity is up to 50%, it could say that maghemite support catalyst can somehow promote isomerization.

Also if hypothesizing that isomerization could be a first step without impeding consecutive APR processes, no further tests were made on magnetic supported catalysts due to: i) the low activity (probably due to low surface area of the support, 8m²/g, and subsequent low Pt dispersion) and ii) due to the reducibility of the Iron oxide support. TPR (Figure 13) and XRD (Figure 14) characterizations indeed confirmed that γ -Fe₂O₃ consume H₂ to form Fe₃O₄ (eq.1).



Figure 13 report the main reduction peak of maghemite at 450°C towards magnetite, but in presence of Pt and Ru the reaction is catalyzed and takes place at lower energy (temperature) thanks to the enhanced H₂ dissociation and spillover capacity of Pt and Ru⁴⁴. From the reduction profile of Pt/ γ -Fe₂O₃ and Ru/ γ -Fe₂O₃, it is observable an asymmetric main peak, respectively at 137°C and 266°C, ascribable to the first reduction of the active phase (eq.2 and eq.3), and the subsequent reduction of the support catalyzed by the metal active phase which facilitate the reduction of the magnetic oxide through a dynamic migration of the absorbed H* from the metal surface. We can hypothesize then that Fe₃O₄ is formed consuming H₂ as soon as it is produced at the reaction condition of our APR.

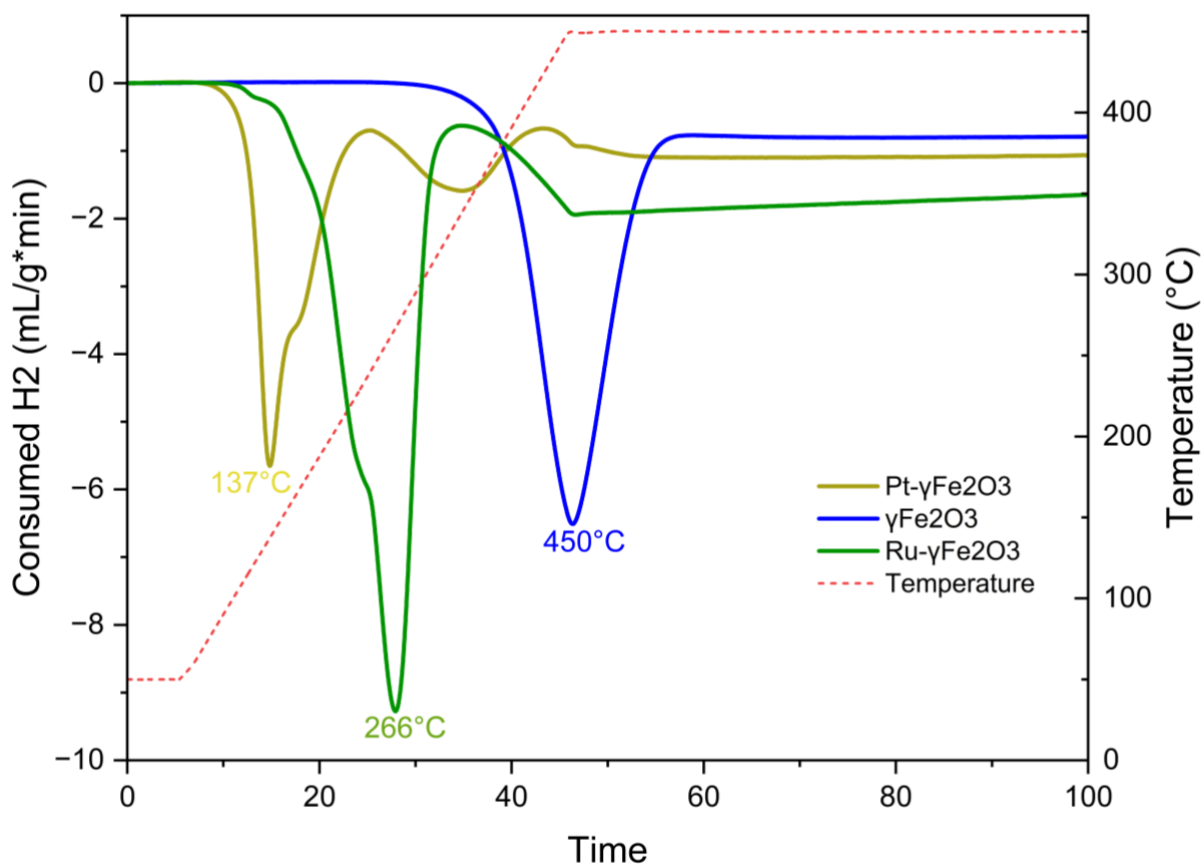


Figure 13 - TPR profiles of maghemite supported catalysts compared to maghemite itself.

The phase composition of the Pt/ γ -Fe₂O₃ (fresh) and the Pt/ γ -Fe₂O₃ (after reaction at 250°C) samples was investigated by X-ray diffraction (XRD) as shown in Figure 14. Magnetite and maghemite are not easy to distinguish at XRD analysis due to their

similar inverse spinel structure, they can be distinguished by a different unit cell measure which shift γ - Fe_2O_3 signals towards higher diffraction angles. In fact, in the oxidation of Fe_3O_4 to γ - Fe_2O_3 the Fe^{II} positions in the inverse spinel are substituted by vacancies which led the unit cell to shrink and γ - Fe_2O_3 to show a defective spinel structure highly magnetic⁴⁵. Another typical difference is the diffraction peak at 18° for Fe_3O_4 which is not present in γ - Fe_2O_3 ⁴⁶. Both the peak at 18° and the shift of the spent catalyst towards lower angle confirmed us the reduction of the magnetic support after the reaction and subsequently, the H_2 consumption of the support.

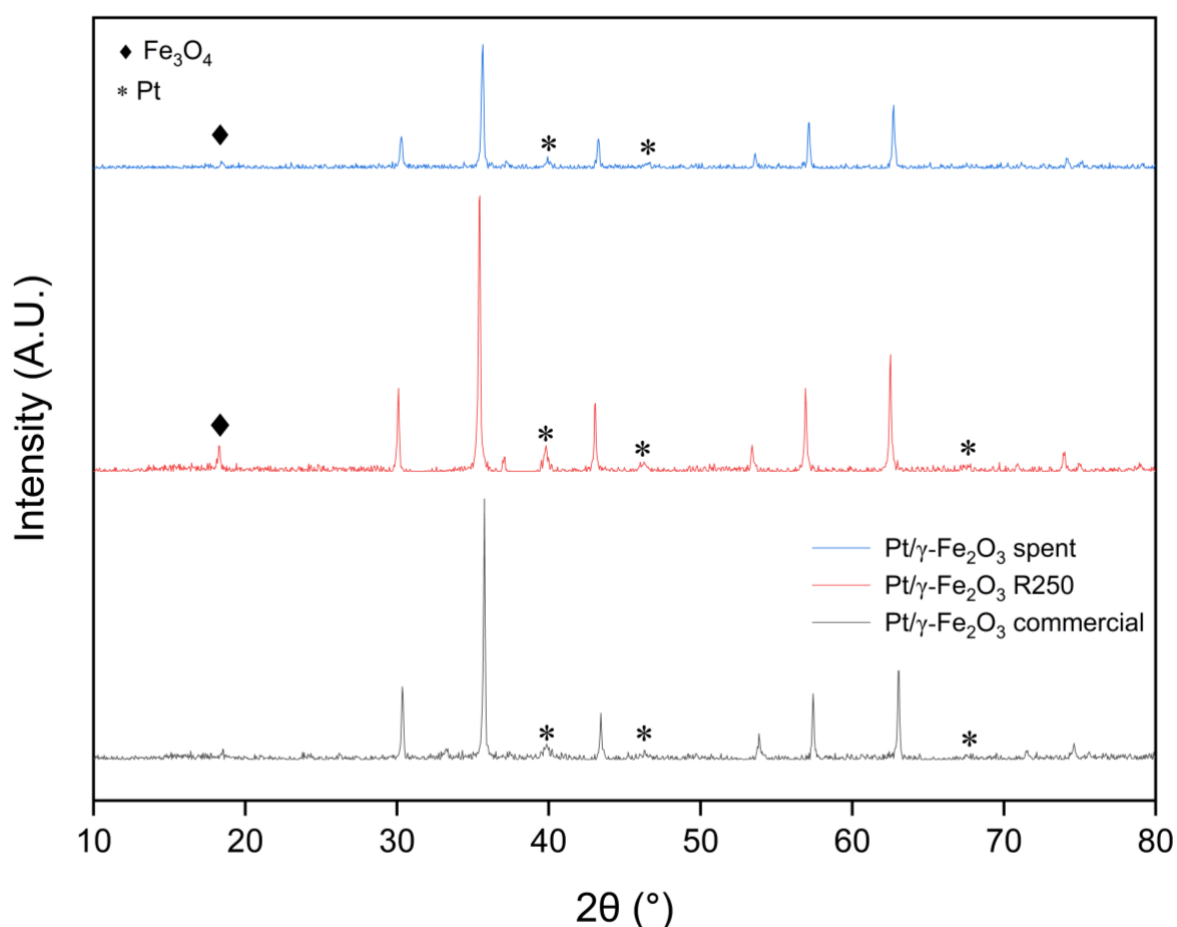


Figure 14 - X-ray diffraction patterns of Pt on iron oxides. (Blue) spent catalyst; (Gray) magnetite - commercial powder; (Red) maghemite obtained by calcination of Fe_3O_4 at 400°C for 3h and reduced at 250°C for 3h with H_2 .

In fact the reduction to Fe_3O_4 doesn't entail any problem for the magnetic recoverability of the catalyst but it means that the already low H_2 producibility is affected by the

reduction of the support. This reduction may weight for a roughly 6 % of hydrogen yield loss.

In summary, maghemite-supported catalysts fail to produce hydrogen satisfactorily, promote mainly isomerization of the feedstock and consumes H₂ for its own reduction to Fe₃O₄. We decided then to change support ignoring the advantages of magnetic properties rewarding higher surface area, the non-reducibility and a different acid and base characteristics.

4.2 Pt supported over metal oxide supports

It is common to use metal oxides as support for reforming catalysts due to their mechanical and chemical resistance under reaction conditions, Al₂O₃ (gamma-Alumina) and MgO are two typical supports that have been studied extensively in the APR reaction.^{47 48 49} The former (Al₂O₃) is characterized by Lewis acids sites which may be hydrated with water finally forming Bronsted sites, this acidity allows an easier metal anchoring on the surface increasing the adsorption efficiency of substrates.³² On the other hand a strong acidity may promote dehydration reactions forming alkenes which may consume hydrogen or lead to catalysts deactivations.⁴⁹ On the contrary, a basic support like MgO, with a strong electron donating behavior, exhibited high hydrogen and lactic acid selectivity as well as low hydrocarbon formation rates, unfortunately its poor stability under hydrothermal condition strongly limit its recyclability.⁵⁰

Making an analogy with the hydrogen yield, it has been reported that binary supports, like mixed oxide, are able to increase the hydrogen production. Mg and Al can be combined in different structures, like stable spinel phases MgAl₂O₄ or coupled in a statistic ordered distribution in a mixed oxide structure through an hydrotalcite precursor. The synthesis of the latter support is the attempt to obtain a material with high surface area and understand the role of acid and basic sites in the reaction, in

particular, we focused on the synthesis of an hydrotalcite precursor with a Mg-Al ratio of 3:1. Hydrotalcite structure consists of three layers, the anion layer (CO_3^{2-}) sandwiched between two layers of metal random allocated Mg-Al hydroxide. During calcination this structure lose water and hydroxyl groups leading to a collapse of the structure towards a homogeneous mixed oxide, moreover CO_3^{2-} in the interlayer is thermally removed as CO_2 from the structure, thus give a high contribution to develop high porosity in the support.⁵¹

4.3 Catalyst Characterization

Catalysts synthesized as described in section 3.2 were characterized for their physical and chemical characteristics. In particular, in table 3 are reported the specific surface area and acid/basic sites for each support.

Support	$S_{\text{BET}}^{\text{a}}$ (m^2/g)	Total NH_3 uptake normalized S.A. (cm^3/g)/(m^2/g)	Total CO_2 uptake normalized S.A. (cm^3/g)/(m^2/g)
Al_2O_3	159.00	0.1271	0.0017
MgAlOx	237.32	0.0037	0.0618
MgO	34.24	N.D.	0.2526

a) Determined by nitrogen adsorption using BET technique. **N.D.**) No detected.

Table 3 -- TPD analysis and N_2 physisorption characterization of different support.

4.4 Catalytic test

4.4.1 5%wt Pt/Al₂O₃

Pt/Al₂O₃ was initially tested as gamma-Al₂O₃ is the most studied support for APR reactions⁵², compared to the previous iron oxide catalyst a large specific surface area of 159 m²/g should disperse Pt better and achieve higher contact area. A higher H₂ production was obtained after 1h respect to Pt/ γ -Fe₂O₃ but, as before, high conversion and low CB underline the role of the acidity of the support which facilitates consecutive dehydration reactions towards unstable intermediates such as furfural and can also result in the formation of humins by polycondensation, which cannot be detected by our analysis system.

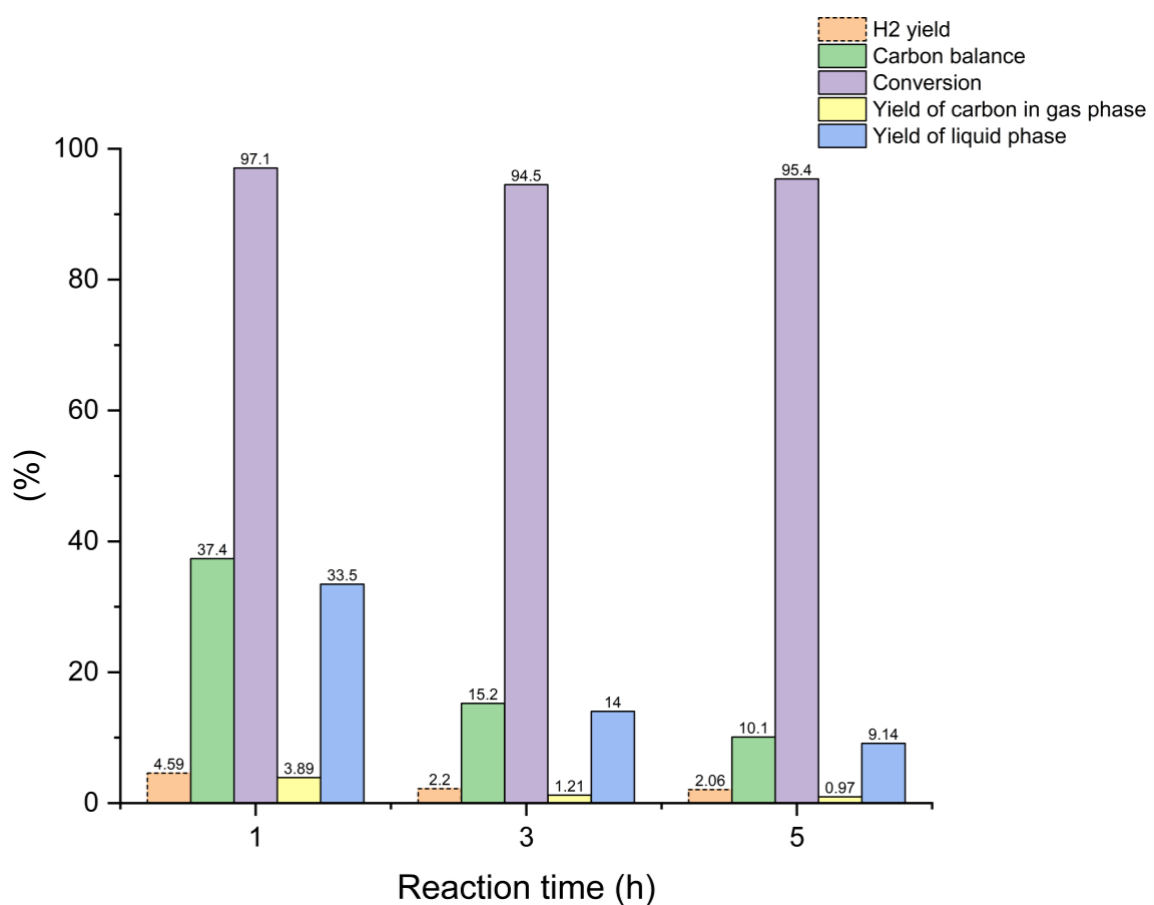


Figure 15 – Catalytic results of the APR of xylitol obtained with 5 wt.% Pt/Al₂O₃ at different reaction time. Condition: 3% wt. of Xylitol, 0.45g catalyst, 250°C.

Tests at higher reaction time were performed and reported in Figure 15 to better understand the reactivity and to eventually favors slower kinetics involved in H₂ production, unfortunately the data underline that the most favorite reactivity is the one which goes towards humin production as confirmed by stable conversion (close to total) while CB steadily decreases with the increase of reaction time, at the same time H₂ yield decrease as well, probably because of the consumption due to the reduction of unsaturated functional groups of heavier side-products (humins). It is reported that add basic additives to Al₂O₃ supports neutralize its acidity and decrease coke deposition on catalyst surfaces by promoting H₂O adsorption and OH surface mobility,⁴⁹ although these strategies could improve catalyst performances, we decided to use directly a different supports.

4.4.2 Comparison between different metal oxide supported catalyst

In order to better understand the influence of acid-base properties on the APR of xylitol different oxide were used as support for the Pt active phase. In Table 4 some reaction parameters are confronted for APR conducted with 5%wt Pt supported over Al₂O₃, MgO and a mixed oxide of Mg-Al with a molar ration of 3:1. Conversion data seems to be pseudo-proportional to the acidity of the support following the order Al₂O₃ > MgAlOx > MgO as well as CB in line with the considerations we deduced from Al₂O₃ tests. On the other hand, besides H₂ selectivity in the gas phase products increase with the basicity of the support, Pt/MgAlOx shows the higher H₂ yield, 25%, these results could be due to the combination of acid-base features of the support or by the higher surface area which may play a role in increasing the dispersion of the Pt active phase.

Catalyst	Pt/Al ₂ O ₃	Pt/MgAlOx	Pt/MgO
Conversion (%)	95.97	66.70	49.14
H ₂ yield (%)	4.59	25.27	13.53
H ₂ selectivity (%) ^a	59.04	68.09	70.88
Yield of C gas phase (%)	3.89	14.34	6.68
Yield of liquid phase (%)	33.46	53.04	77.94

A mass of catalysts is the same 0.45g. The Pt loading is 5 % on supports.

^a: molar fraction of H₂ in the gas phase

Table 4 - Comparison of three catalysts by APR of 3% wt. of Xylitol at 250°C with 1h

Considering the promising results obtained Pt/MgAlOx has been used for kinetic tests to maximize H₂ production and tests on reaction intermediates have been performed to better understand the reaction pathway over these materials.

4.4.3 Reaction mechanism investigation

The liquid phase derived by the APR of xylitol is a complex mixture, a high number of side reactions can occur during the reaction towards a vast range of shorter chain products. APR tests on shorter polyols were planned to simplify the final reaction mixture and, basically, limit the possible reaction pathways, in this regard APR results on glycerol and xylitol are compared in Figure 16.

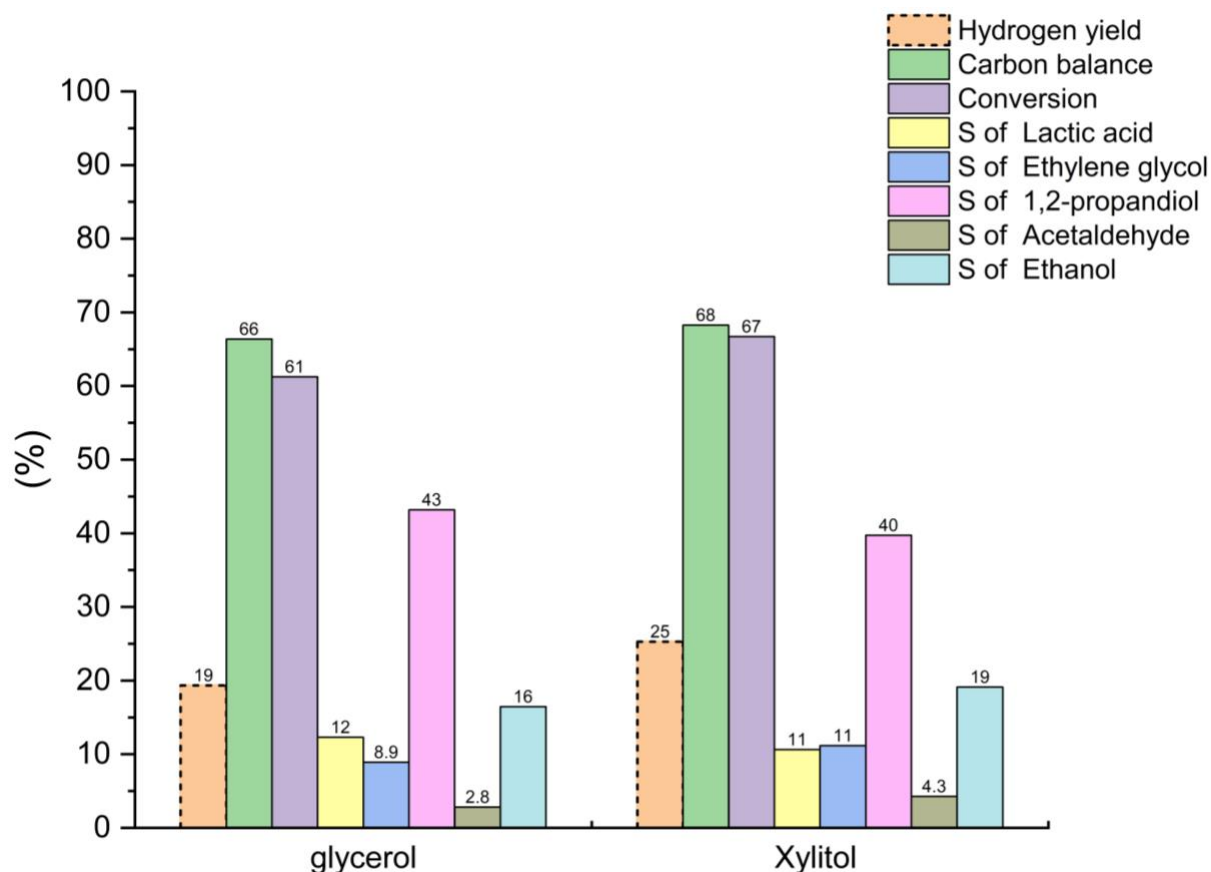
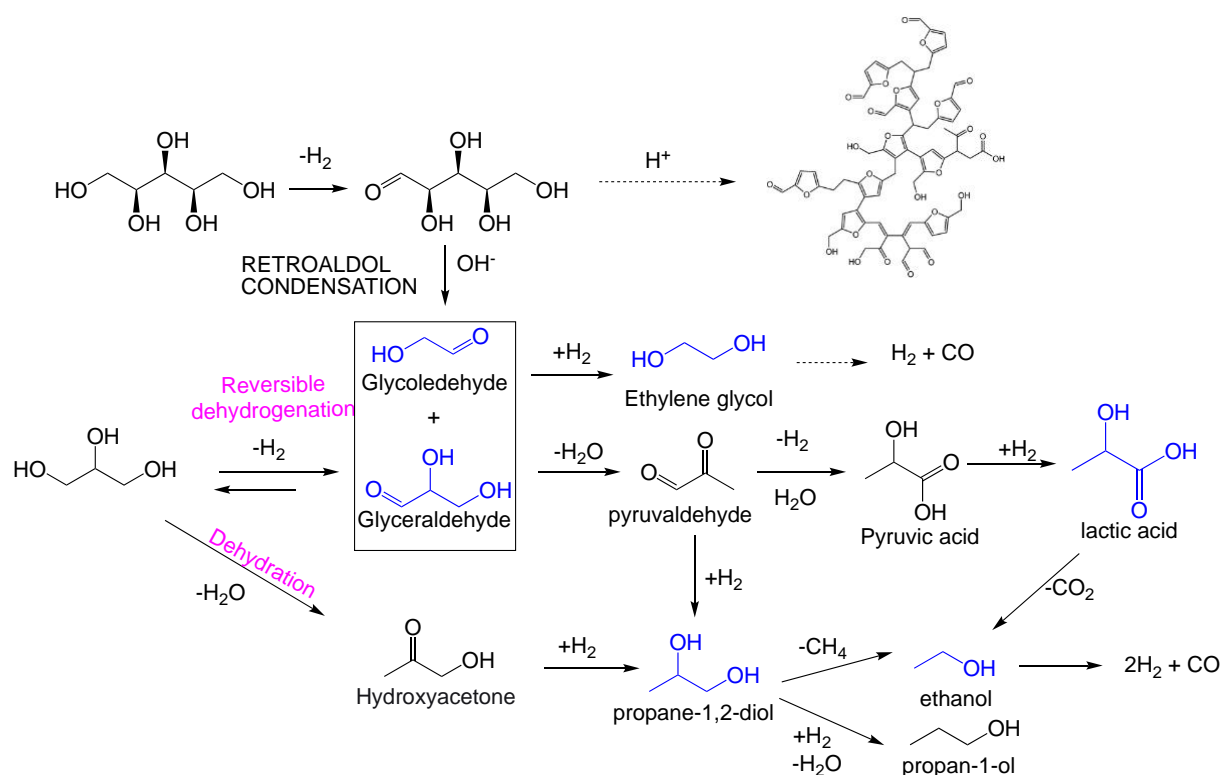


Figure 16 – APR results obtained starting from glycerol and xylitol. Condition: 0.45g of Pt/MgAlO_x, 250 °C, 1h and the same quantity of feedstock (0.01mol in water)

Interestingly, by changing the substrate moving from xylitol to glycerol very similar results have been obtained not only in terms of substrate conversion values, CB and H₂ yield but also considering the products distribution in the liquid phase, suggesting some insights on the reaction mechanism. A similar product distribution from those different chain-length feedstocks could be explained by a highly effective primary retro-aldol reaction on the xylitol catalyzed by the basic sites of the support. As explicated by the scheme of reaction reported in Scheme 3, after a first dehydrogenation to xylose, the chain is shortened to glycolaldehyde (C₂) and glyceraldehyde (C₃) through retro aldol reaction, from these two intermediates we hypothesized a whole reaction pathway which found in the glyceraldehyde a common intermediate with the glycerol APR pathway. In fact, if the glycolaldehyde (C₂) is more easily converted towards ethylene glycol and then to H₂ and CO, longer chain like C₃

glyceraldehyde can undergo different pathways²⁶ towards the main products listed in Figure 16 and colored in blue in Scheme 6. In particular one of the main route we hypothesized is a dehydration of the glyceraldehyde towards pyruvaldehyde which can be hydrated and hydrogenated towards lactic acid passing through pyruvic acid. Another pathway we confirmed foresee a reversible hydrogenation of glyceraldehyde to glycerol and a dehydration to hydroxyacetone followed by hydrogenation to 1,2-PDO, alternatively glycerol can dehydrogenate on the more coordinated carbon to form dihydroxyacetone, instead of glyceraldehyde, which can be dehydrated as well towards pyruvaldehyde route described before. 1,2 PDO and lactic acid, as key intermediates, can then be converted to H₂ and CO₂ passing through ethanol formation or undergo hydrogenation towards 1-propanol.



Scheme 6 – A possible reaction pathway for the APR of xylitol in the presence of Pt/MgAlO_x at 250 °C, Blue compound is detected by HPLC.

Hydrogenation and dehydrogenation reactions take place catalyzed by the Pt active phase, as well as C-C cleavage, in the same reaction environment basic catalyzed reaction takes place on the predominant basic sites of the support (Mg:Al 3:1) while

acid catalyzed reaction are mainly favored by homogeneous catalysis due to the presence of organic acid in solution, also the mixed oxide has some acidity due to the presence of Al in the MgO lattice. Nonetheless is a weak acidity. Scheme 7 shows the APR pathway of xylitol considering acid and base catalyzed mechanisms of reaction, both scheme commonly foresee a first xylitol dehydrogenation to aldose and ketose sugars to enable cleavage reactions, due to the strong adsorption through the formation of Pt-C bond or Pt-O bond.²⁶ Furthermore, if a formed ketose desorbs and re-adsorbs, then epimerisation can proceed via reversible (de) hydrogenation alone. Depending on the employed reaction conditions (i.e. alkaline or Lewis acidic), aldose and ketose sugars can be interconverted through the Lobry de Bruyn–Alberda van Ekenstein (LBE) reaction.⁵³ These reactions are reported to result mainly in the formation of two isomers arabitol and ribitol, with arabitol as the major product⁵⁴, and probably those are the mechanisms involved on the initial magnetic catalysts we tested. At this point the conversion can proceed with a similar pathway from arabitol to threitol and erythritol by decarbonylation and dehydrogenation, further cleavage of C-C and C-O bonds could lead to the production of EG, 1,2-PDO, GLY, butanediol (BDO) and CH₄.

Regardless of an initial isomerization, analyzing the acid catalyzed process, the main mechanism is dehydration of the internal hydroxyl groups and activation of formed carbonyl C-O bond, which undergoes further hydrogenation. Alkanes production is also favored, carbonyl groups tend to be dehydrated and hydrogenated, as well as carboxylic acids tend to be decarboxylate; CH₄ is likely to be produced by ethanol dehydrogenation in the formation of aldehydes that finally formed CO₂ and hydrogen by decarboxylation and WGS. As demonstrated in precedence this type of catalysis compete with humin formation by polycondensation which is favored by long time of reaction, higher temperature and higher feedstock concentration.⁴⁷

Under basic conditions, the retro-aldol mechanism decomposes C₅ into C₃ and C₂ on the basic site, then C–C bond cleavage underwent to form adsorbed CH_yO species

which could be dehydrogenated to form adsorbed CO. the adsorbed CO was removed by WGS reaction to produce CO₂ and H₂. Otherwise, desorption of adsorbed CO led to the formation of gaseous CO.⁴⁸ As said before, due to the complex reaction environment and to the many different catalysis offered by the catalyst or the reaction environment, many mixed pathways are possible and here hypothesized to explain the presence of the main liquid phase products.

4.4.4 Optimization of the reaction condition with Pt/MgAlOx

In order to maximize H₂ yield, tests at different reaction time were performed at 250°C using Pt/MgAlOx catalyst, these tests were performed to better understand the kinetic of the process (Figure 17). Indeed, H₂ production tends to increase as time of reaction increases, reaching a maximum of 33% with an 80% of conversions at 3 h. Subsequently the H₂ yield decreases, due to hydrogen consumption from parasite reaction on heavy compounds formed in the liquid phase like humins which are favored at higher time of reaction (CB slightly decrease increasing time of reaction). One possible explanation is also due to catalyst deactivation, it is reported that MgAlOx in aqueous media can turn back to a hydrotalcite like structure due to a material memory effect⁵⁵, thus would change the surface characteristics of the support leading to a possible different reactivity (detail discussed in the sequent chapter).

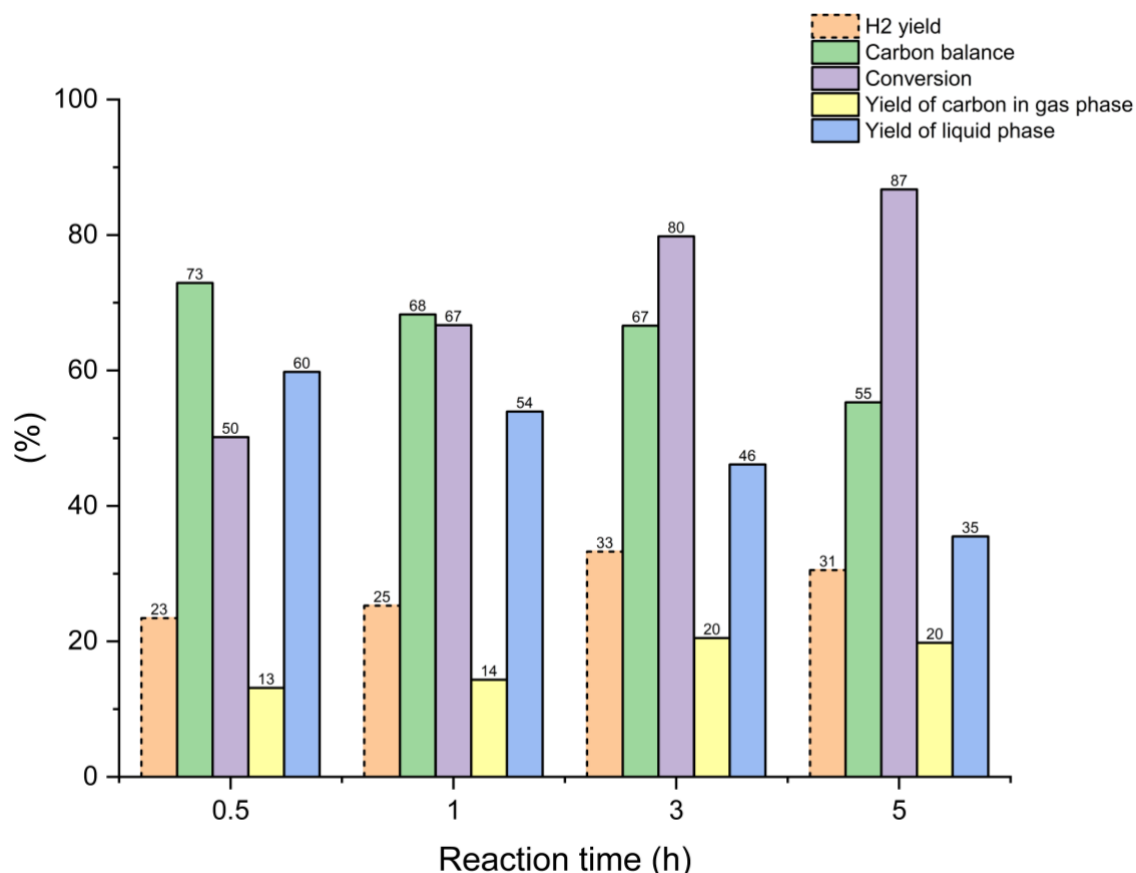


Figure 17 - - Catalytic results obtained at different reaction time for the APR of xylitol with 5 wt.% Pt/MgAlOx Condition: 3% wt. of Xylitol, 0.45g catalyst, 250°C.

In graphics are also reported the distribution of products detected in gas and liquid phase, calculations were made considering the carbon content of every product and referring every yield and selectivity to the carbon content of the initial feedstock. Interestingly, yield of C-containing molecules in the gas phase is proportional to the H₂ yield, in fact hydrogen is co-produced with CO₂ at a close to constant ratio that is around 0.44 (which is why H₂ selectivity is almost constant in every reaction). This ratio, as well as H₂ selectivity and productivity is depicted in Table 5. Figure 18 shows the distribution in terms of molar fraction of both the gas and the aqueous phase. All these data clearly show the absence of CO suggesting the very high efficiency of our catalytic system in promoting WGS reaction towards CO₂ (selectivity ~90%) and H₂. The latter is partially consumed via methanation (CH₄~10%) while only trace of light alkanes resulted in the final gas composition. On the other hand, H₂ shows a selectivity between 65 and 68% and selectivity with CO₂ and CH₄ of respectively 28-30.5% and 3.33-3.87%. In Figure 19 shows the composition of gas phase that could provide more information for industrial application, in particular we obtained gas streams containing more than 40%mol of H₂.

In the liquid phase we observed a high presence of 1,2-PDO, LA and EG in every test while 1-propanol raise with reaction time (in combination with H₂ and Lactic acid consumption) while EtOH seems to reach a peak at 3h and be quite totally consumed (probably towards H₂) at 5h, we hypothesized that this H₂ is mainly consumed (which find evidence in the higher molar ratio of CO₂/H₂).

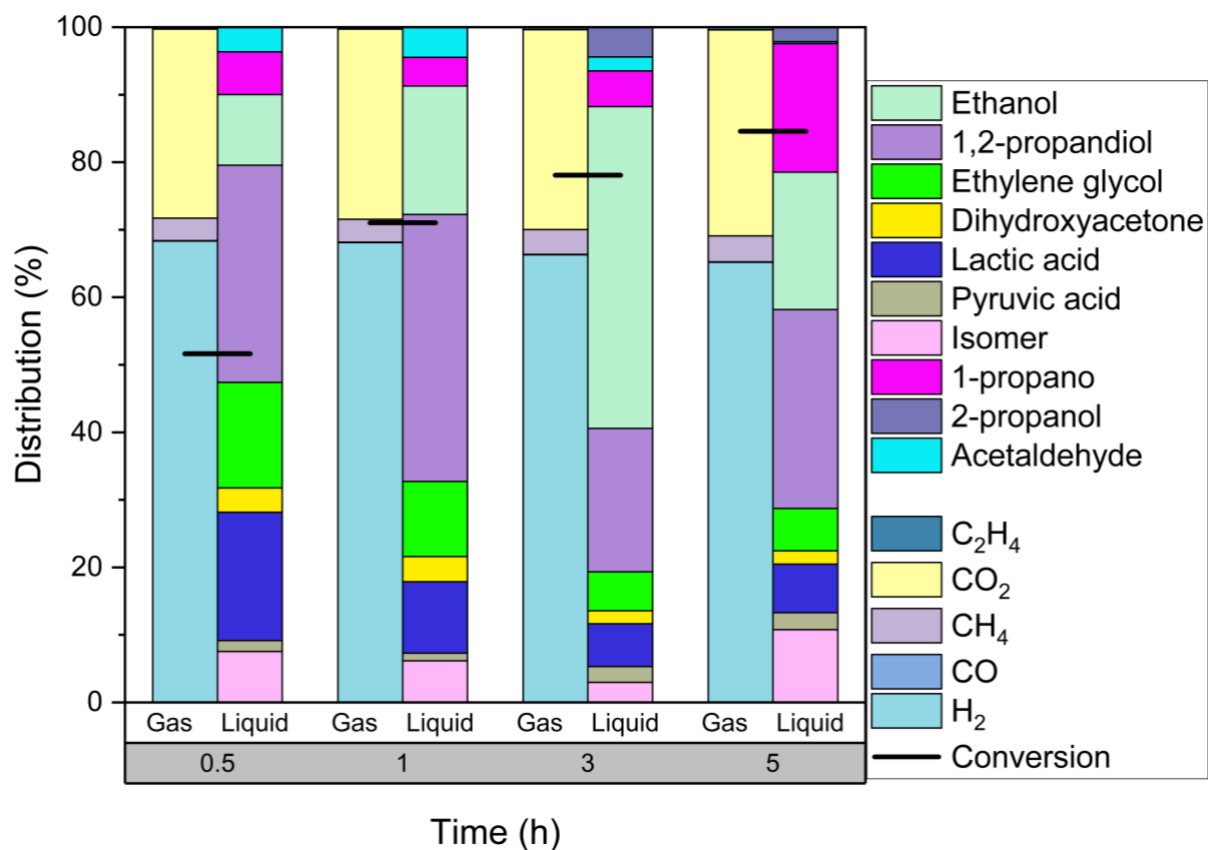


Figure 18 - Products distribution of different reaction time. Condition: Condition: 3% wt. of Xylitol, 0.45g catalyst, 250°C.

	S _{WGS}	S _{CH₄}	CO ₂ /H ₂	Productivity (mmol H ₂ /g)
0.5h	89.19	10.61	0.41	31.37
1h	89.06	10.73	0.41	33.42
3h	88.82	11.04	0.45	44.15
5h	88.63	11.24	0.47	33.43

Note: for WGS complete CO₂/H₂ = 0.4545. S: selectivity.

Table 5 – The comparison of gas phase in different reaction time.

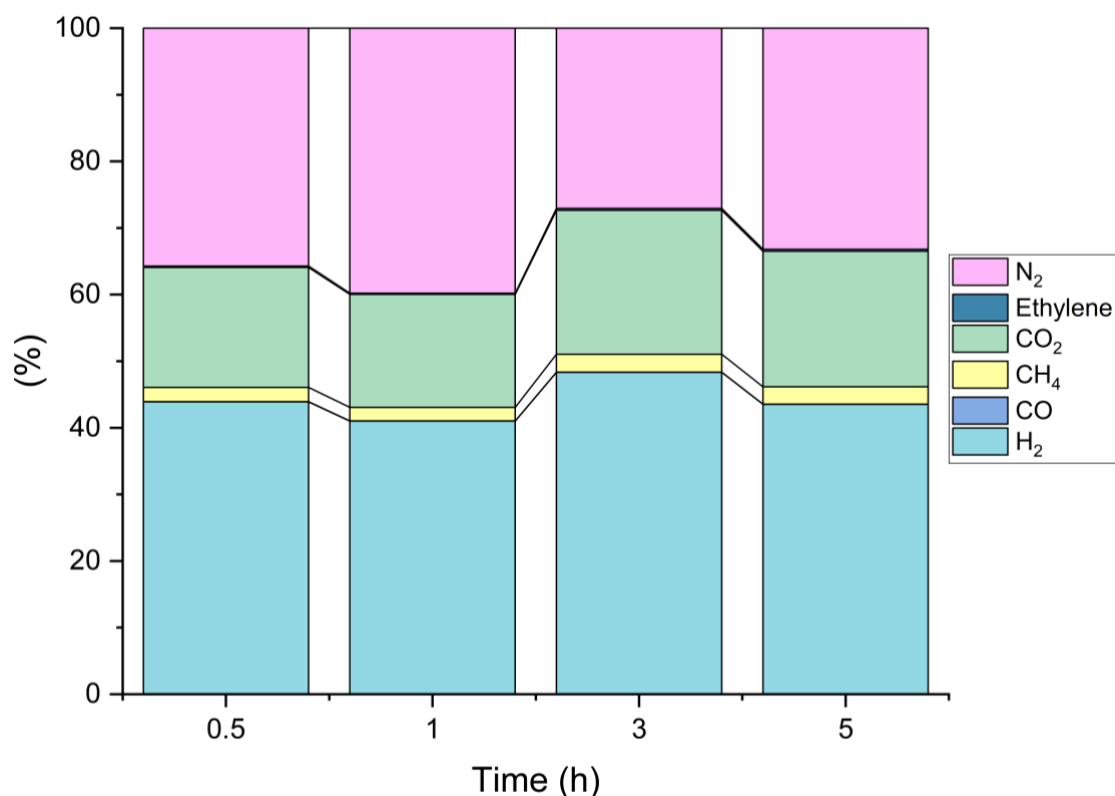


Figure 19 - Composition of gas phase after reaction calculated as molar fractions taking into account also the initial nitrogen pressure loaded at RT.

As the best results in terms of H₂ yield was obtained at 3h in the previous test we investigated the reaction temperature keeping the optimized reaction time, in order to eventually reach a similar yield at milder conditions. Unfortunately, Figure 20 shows that in terms of H₂ yield the reaction is strongly favored at 250 °C, this energy is probably needed to favor the activation of WGS and many C-C cleavage pathways while lower reaction temperature led to parasite reactivity in liquid phase, C-C cleavage mainly through retro aldol reaction, but with low gas product development and lower conversion of C5 xylitol.

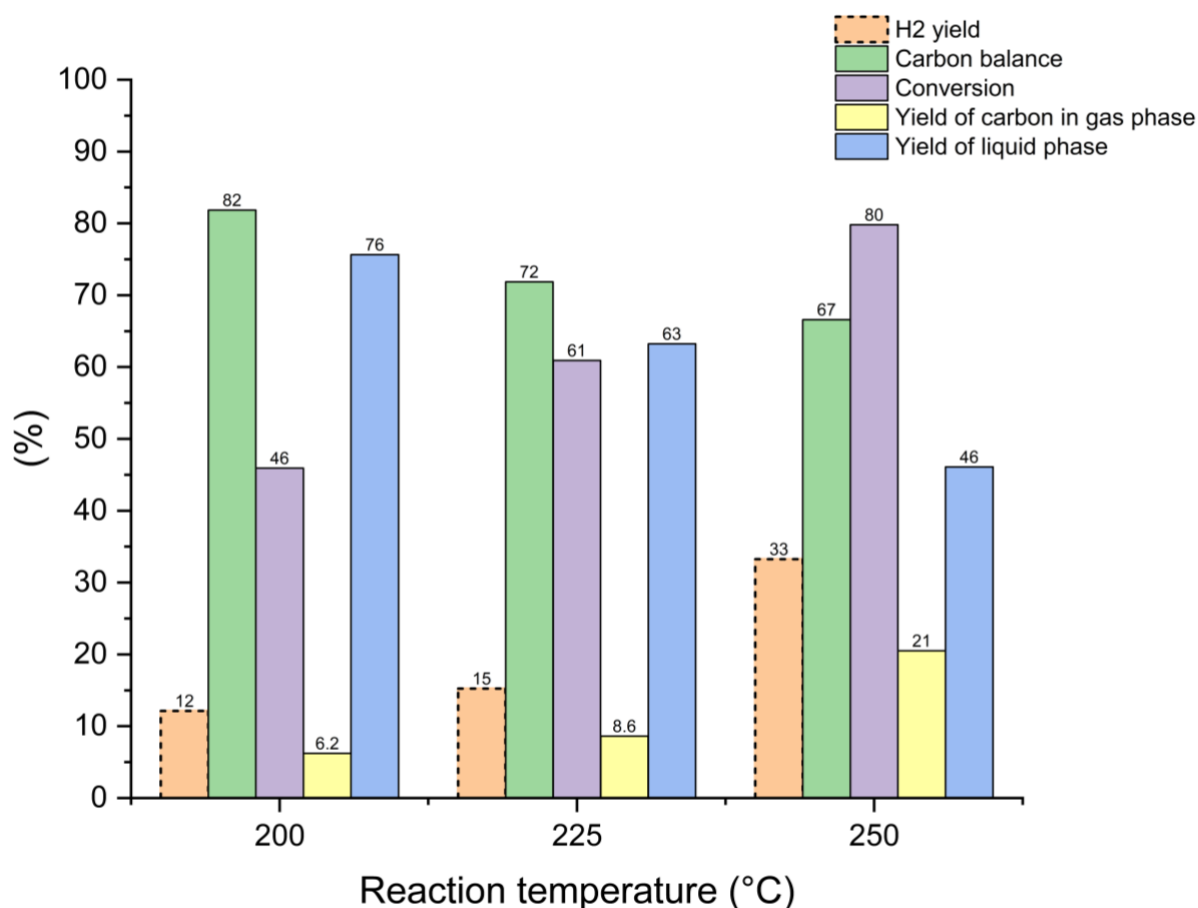


Figure 20 - Different temperature with 5 wt.% Pt/MgAlOx. Condition: 3% wt. of Xylitol, 0.45g catalyst, 3h.

4.4.4.1 Spent catalyst characterization

In order to better understand the industrial potential of the catalytic system we developed; X-Ray diffraction analysis has been performed on the spent catalysts derived from the kinetic tests previously reported. XRD patterns reported in Figure 21 are strikingly similar to those of a synthesized MgAl-hydrotalcite. Specifically, diffraction peaks located at 2θ ($^\circ$) = 11.5, 23.3, 34.7, 38.7, 45.8, 60.6 and 61.8 are attributed to an hydrotalcite structure or a layered double hydroxide (LDH) (similar structure). Among them, the peaks located at 11.5°, 23.3° and 34.7° correspond to the (003), (006) and (009) planes, which confirm the formation of well-defined crystalline sheets with rhombohedral symmetry.⁵⁶ Peaks not attributed to the LDH structure are allocated at 18.3°, 37° and 60.5° and correspond to Mg(OH)₂. With reaction time

increasing, $\text{Mg}(\text{OH})_2$ presence increase, this is probably due to the dissolution of part of the Mg on the LDH structure, thanks to mild acidic pH of solution due to the coproduction of organic acids ($\sim 4,5$) which can eventually reprecipitate as $\text{Mg}(\text{OH})_2$.

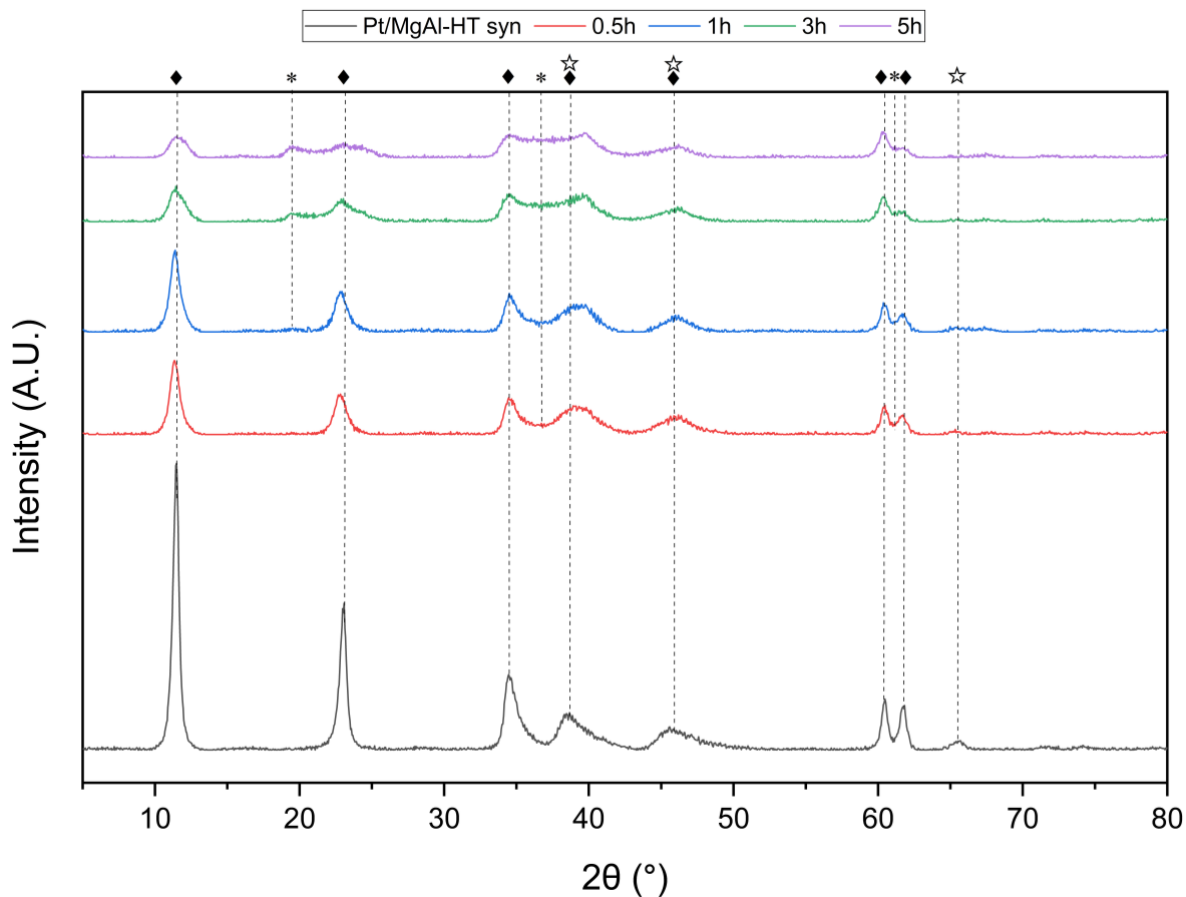


Figure 21 - X-ray diffraction patterns of the Pt/MgAlOx with different reaction time at 250°C. Pt/MgAl-HT syn is not calcinated, others are Pt/MgAl-HTics after reaction (spent) at different reaction time. [♦] MgAl-HT, [*] Brucite, $\text{Mg}(\text{OH})_2$ and [☆] Pt.

Already after 0.5 h of APR condition the mixed oxide change its structure toward a LDH/HTics structure, we then decided to test this spent material to investigate his eventual deactivation for the APR of xylitol.

According to the XRD patterns, the intensity of HT decreases with increasing reaction time, while after 3 hours the presence of brucite is evident. The unit cell parameter (d spacings) is the distance between two metal ions within the layers. However, the distance between MgAl-HTics is smaller than MgAl-HT (7.75 \AA), it is only over 3 hours

(7.72 Å) that the gap of distance can be observed. At 5h the gap of d spacing is the largest for 7.68 Å, and less than 3 hours is not apparent.

4.4.4.2 Recycle test

On industrial scale, heterogeneous catalyzed processes need to foresee a catalyst quantitative recovery and, possibly, its activity over multiple cycles of reaction, eventual loss of catalyst material and/or activity could strongly affect on an economic potentially interesting process. Despite the change in the catalyst structure, verified through XRD analysis, we decided to test the recycling potential of our material charging the spent catalyst, collected after a cycle of APR, with fresh xylitol to repeat the test and simulate an industrial recycle of the material. This operation was repeated a second time in order to obtain an activity profile for 3 reaction cycle. No specific intermediate washing steps or regeneration of the material have been performed between the reaction cycles.

The reaction conditions kept for the tests were the previously optimized 3h reaction time at 250°C, in the results reported in Figure 22, the H₂ yield obtained at the 1st reaction cycle (i.e. over the fresh material) reaches 39%, the value is higher than the 33% obtained in the previous tests. The reason can be found in the physical difference of the support, in fact the hydrotalcite precursor had to be re-synthesized and, besides we repeated the same synthesis, the second batch, used for the now reported recycle tests, showed higher surface area (237 m²/g instead of the previous 199 m²/g). Thus, could explain a higher activity due to higher contact surface of the catalyst and eventually a different dispersion of Pt. Despite the structural change demonstrated by the XRD of the spent catalysts used in the kinetic tests, the Pt/MgAl-HTlcs surprisingly continued to show quite-constant H₂ yield for the 2nd and 3rd times reaction. The distribution of products, the Figure 23 and Table 6, confirmed the coproduction of CO₂ and H₂ also for the recycle tests in close to theoretical ratio (also if slightly lowered by

the higher yield of H₂), at the same time also WGS and methanation selectivity seems in line with the previous tests. Figure 24 shows the molar fraction composition of the gas phase underlying a H₂ concentration close to 50% for each test.

Considering the aqueous phase, xylitol conversion was steady at around 90%, the main products are still represented by lactic acid (LA), ethanol, 1,2-PDO and 1-propanol, raising the cycle of reaction led unfortunately to undetected products which result in lower CB and lower selectivity towards valuable products. The pH of the 3rd cycle reaction mixture results to be 4.5 instead of 7 after the 1st cycle, thus led us hypothesize that the unknown products previously cited could be the major responsible for this change of the acidity of the solution. From these considerations we decided to investigate more in deep the transformation of the catalyst during the cycles of reaction and to characterize the spent materials.

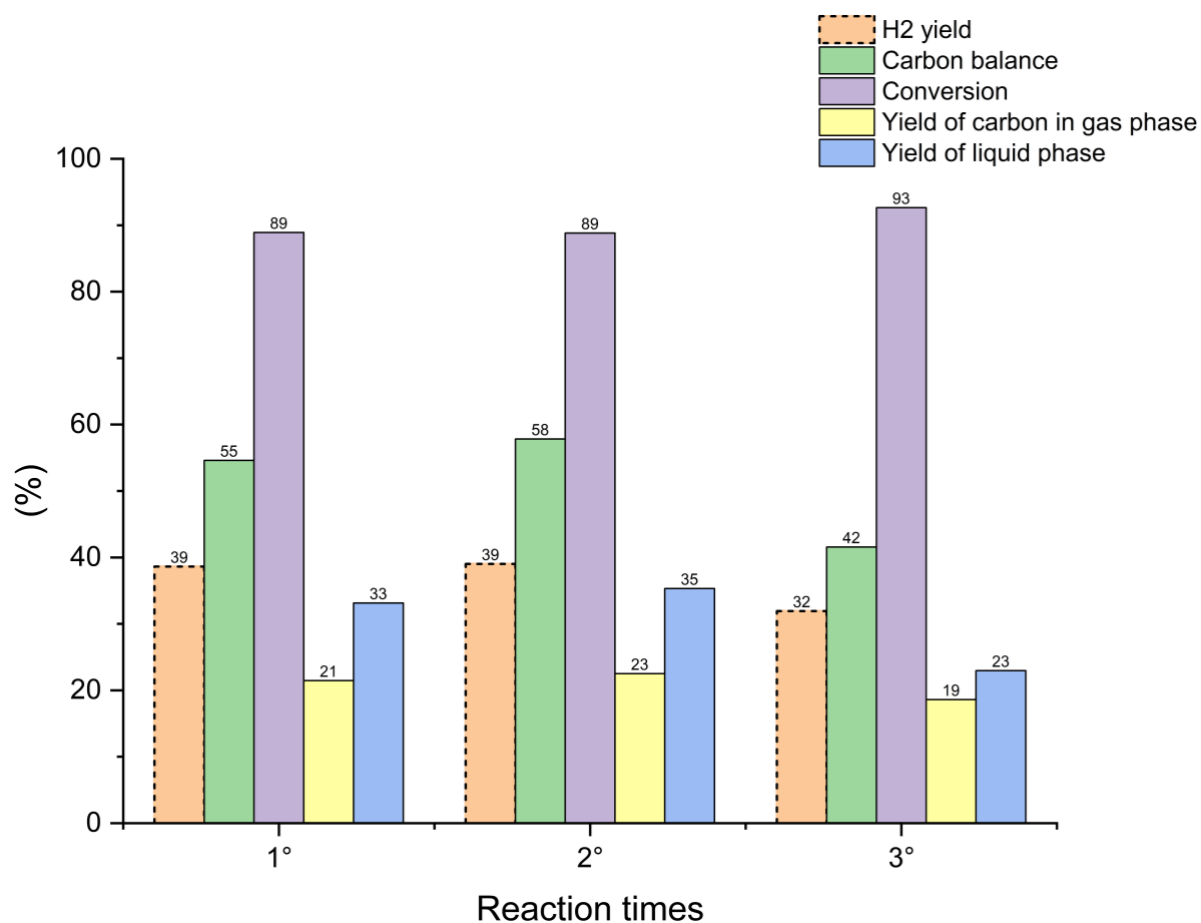


Figure 22 – The recycle test result. Condition: in 1^otime reaction with, 0.45g of 5 wt.% Pt/MgAlOx. 3% wt. of Xylitol, 3h, 250°C. 2^otime reaction with spent catalyst of 1^otime reaction, 3% wt. of Xylitol, 3h, 250°C. 3^otime reaction with spent catalyst of 2^otime reaction, 3% wt. of Xylitol, 3h, 250°C. Between two reactions, the spent catalyst was just washed with water without any other treatment.

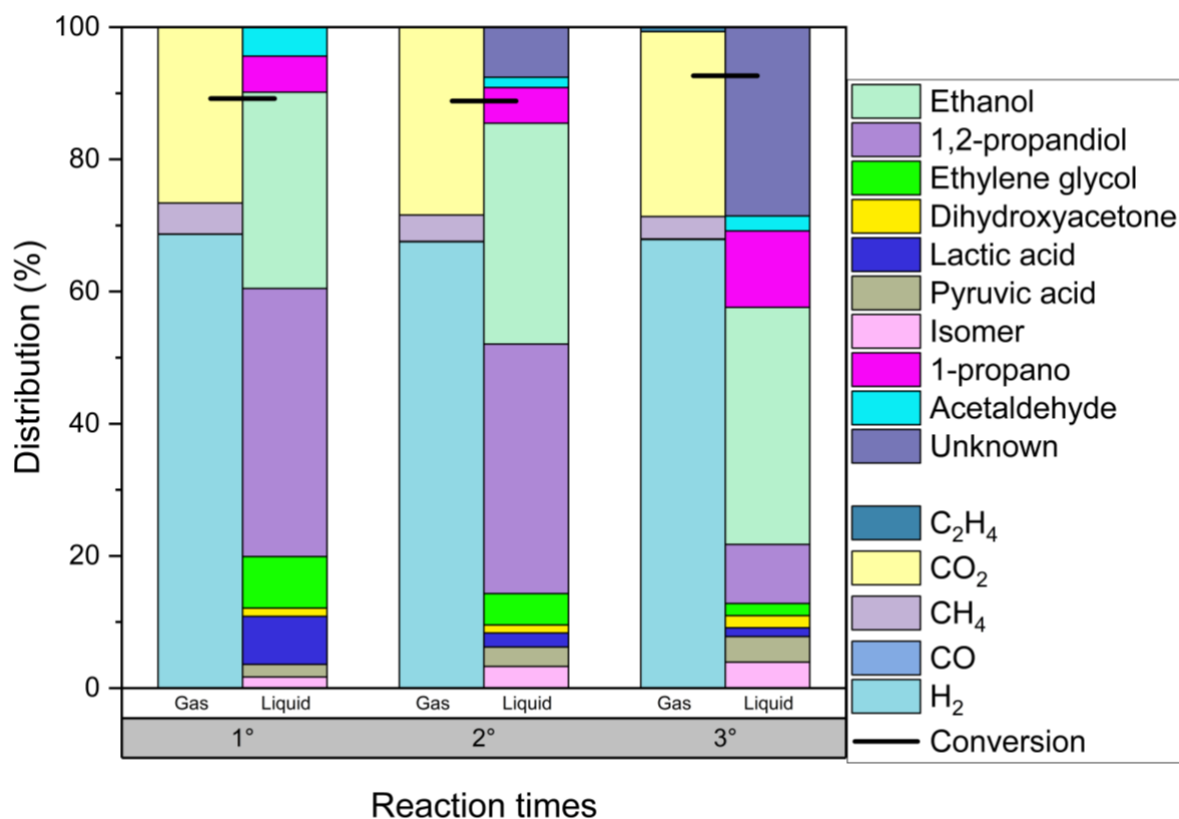


Figure 23- Products distribution of three different times reactions. Condition: in 1^otime reaction with, 0.45g of 5 wt.% Pt/MgAlOx. 3% wt. of Xylitol, 3h, 250°C. 2^otime reaction with spent catalyst of 1^otime reaction, 3% wt. of Xylitol, 3h, 250°C. 3^otime reaction with spent catalyst of 2^otime reaction, 3% wt. of Xylitol, 3h, 250°C. Between two reactions, the spent catalyst was just washed with water without any other treatment.

	S WGS	S CH ₄	CO ₂ /H ₂	Productivity (mmol H ₂ /g)
1°	85.01	14.94	0.39	55.41
2°	87.51	12.34	0.42	32.09
3°	88.93	10.82	0.41	32.34

Note: for WGS complete CO₂/H₂ = 0.4545. S: selectivity.

Table 6 -- The comparison of gas phase in different reaction times.

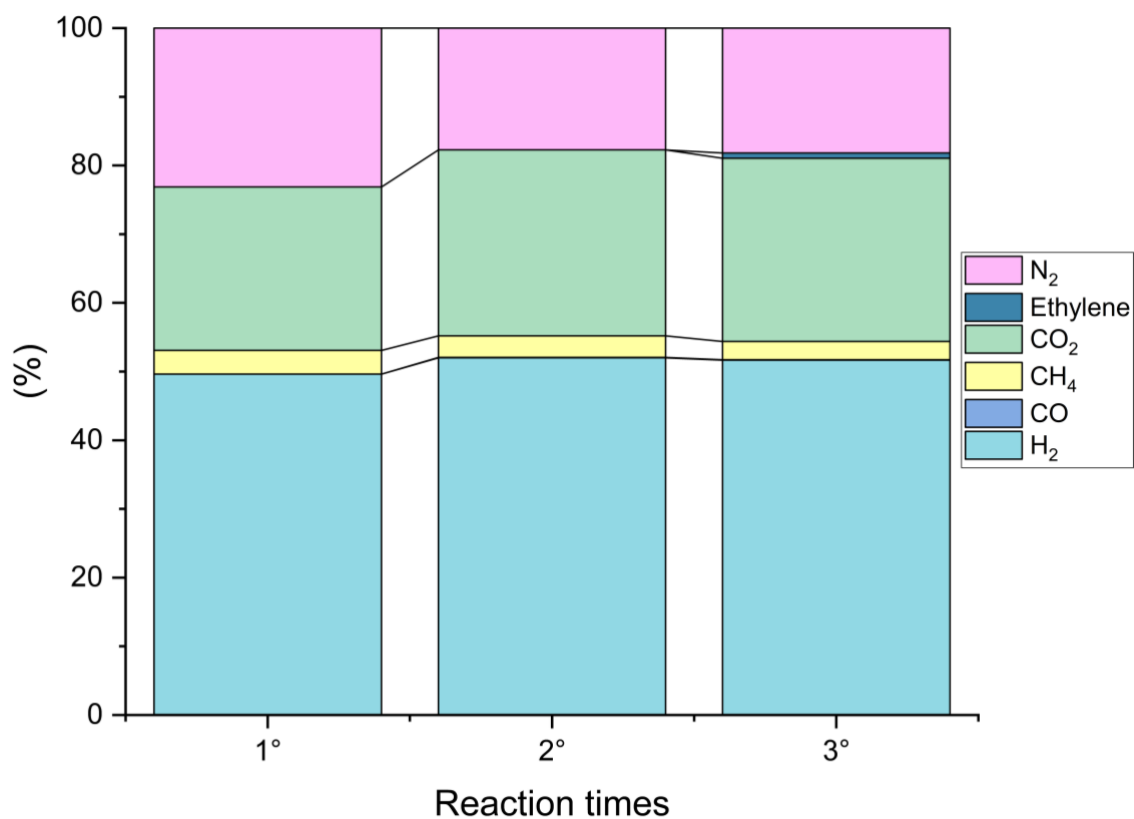
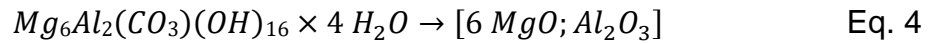


Figure 24 – Composition of gas phase after reaction calculated as molar fractions taking into account also the initial nitrogen pressure loaded at RT.

As noticed also during the kinetic tests, the amount of catalyst collected at the end of the APR result higher than the initial quantity charged in the reactor. This is explainable by the already mentioned transformation of the mixed oxide towards HTlcs materials

which have a higher molecular weight. In eq.4 is reported the stoichiometry of the HT calcination to mixed oxide.



MW_{HT}=604 g/mol; MW_{MO}=304 g/mol

Based on this equation we expect a total mass loss of 44.4% to obtain, completely, the mixed oxide structure. In fact, the material is expected to undergo: (1) loss of the H₂O of crystallization (weight loss of roughly 12%wt); (2) CO₂ development from the decomposition of the interlayer carbonate (ca. 10%wt); (3) dehydration of hydroxides with the formation of metal oxide structure: 16OH→8H₂O (ca. 22.5%wt).

TGA analysis (Figure 25) was performed on the as synthesized HT and on the spent HTIcs derived from the 3^otime reaction to verify the similarity of the materials. Synthesized HT undergo a total mass loss of 44.4%, as predicted theoretically by the stoichiometry of the reaction, moreover it confirmed that the calcination conditions adopted in this work are sufficient to achieve the mixed oxide structure. The characteristic loss of crystal water is observed at approximately 205-220°C while the dehydration and CO₂ development took place from 300 to 400°C leading to the mixed oxide structure.

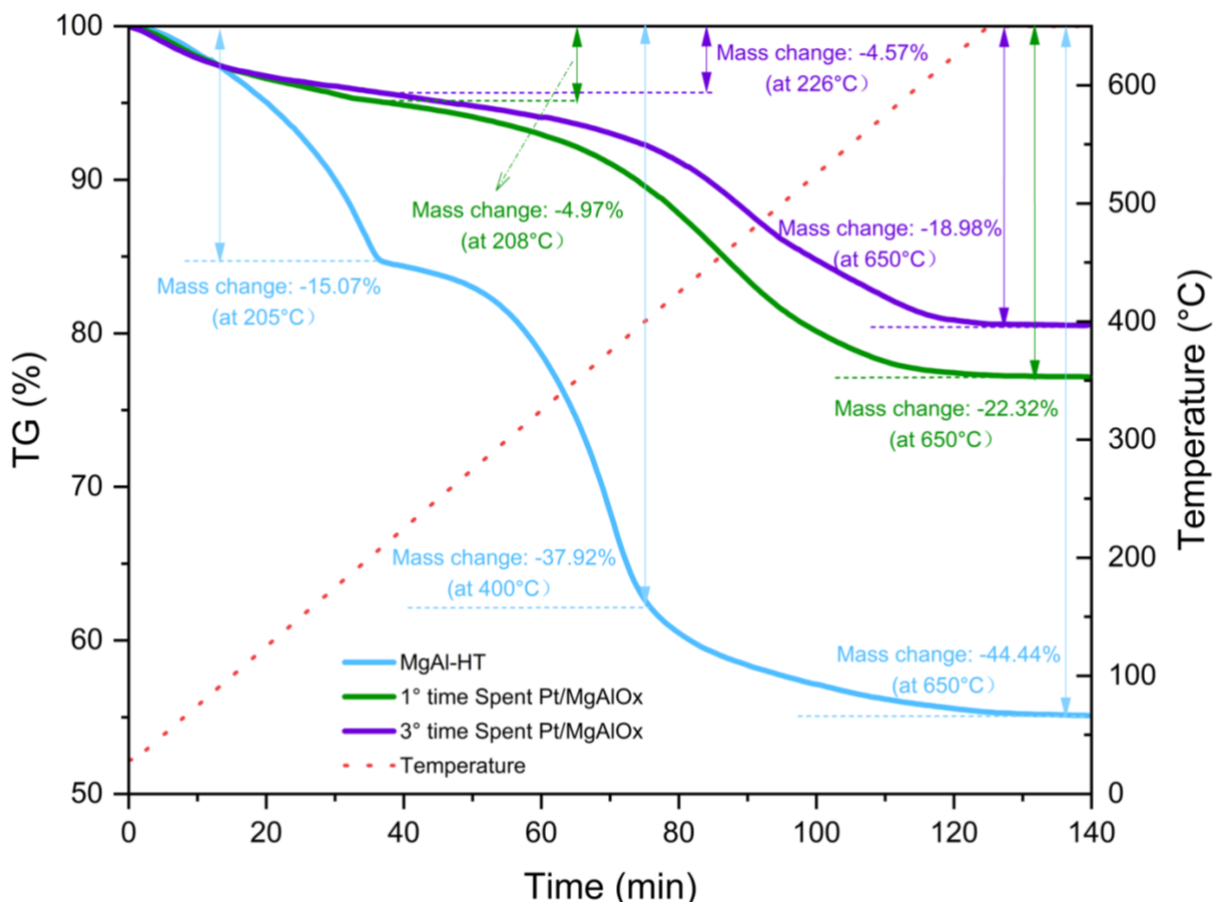


Figure 25 – TG curves for MgAl-hydrotalcite (blue line), 1° time reaction spent Pt/MgAl-HTlcs (green line) and 3° time reaction spent Pt/MgAl-HTlcs (purple line).

The TGA of both the spent catalysts underline a minor mass loss then the synthesized HT, that could be explained by a minor water content (~10%wt difference) and a LDH structure instead of the HT. A significant rearrangement of the mixed oxide towards HTlcs happens, but without the adsorption of an interlayer anion, this transformation led to a double layered hydroxide structure which explain the remaining 10% wt difference in the mass loss analysis (due to the absence of CO_3^{2-}). Moreover, the absence of other substantial mass loss in the range of 550°C underline that no solid by-products are deposited on the catalyst surface, this eventual deactivation behavior is excluded for at least three reaction cycles.

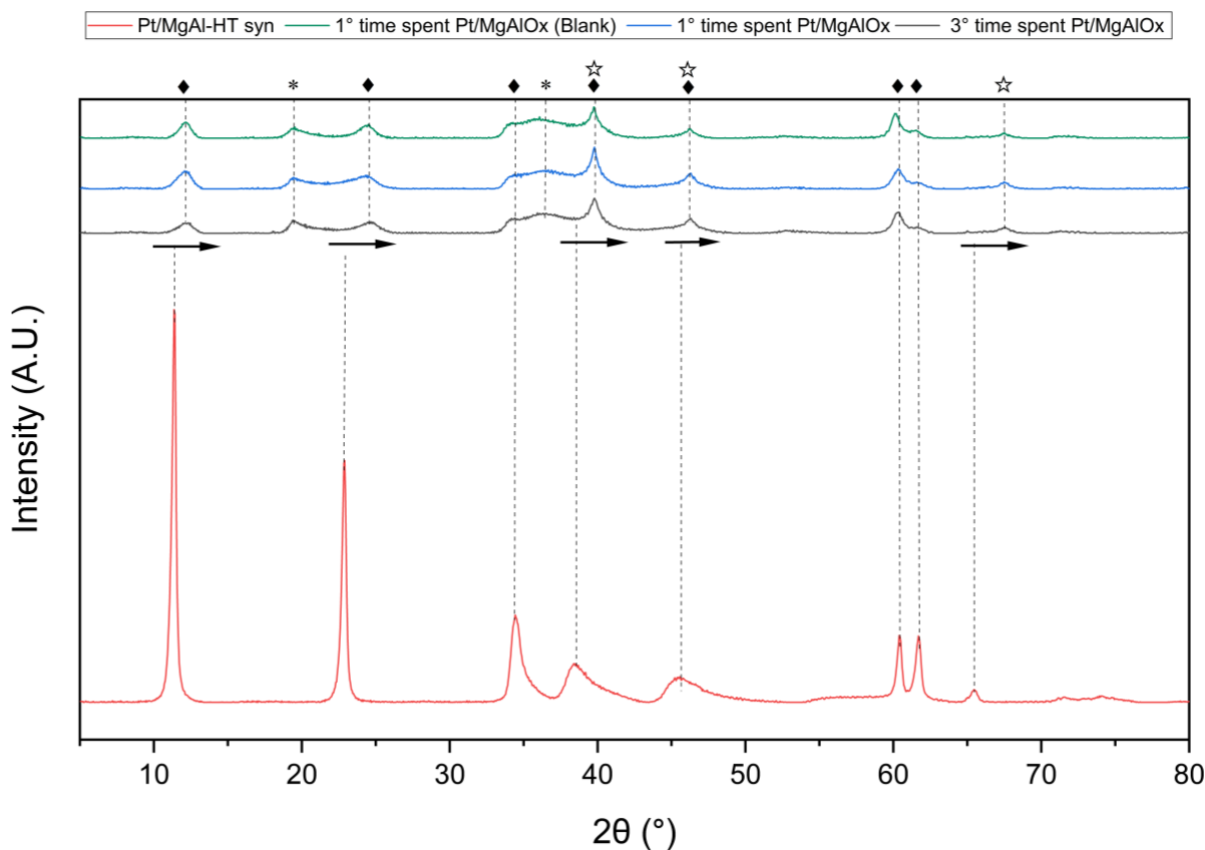


Figure 26 – X-ray diffraction patterns of the Pt/MgAlOx with different cycle times at 250°C. [◆] MgAl-HT, [✱] brucite, Mg(OH)₂ and [☆] Pt.

As underlined in XRD analysis reported in Figure 26, respect to the synthesized HT, the blank test of spent catalyst and the spent catalyst shows a lower d spacing, because the pattern of spent catalyst shifts toward right that means the lattice decreases with increasing reaction times and HTICs in fact have less void space in their interlayers and can eventually lose activity because they have less contact with the reagents⁵⁷.

The spent catalysts were also characterized by TPD analysis and physisorption, as reported in Table 7. The total acid sites resulted to be lower than the basic sites, as expected for a Mg/Al ratio of 3:1, and they result to be moreover unchanged after a cycle of reaction while they both drastically raise after the 3^otime reaction. Another observable effect is linked with the surface area, which decrease to 173 m²/g after the 1^otime reaction and raise again after the 3^otime reaction. This effect could be explained by the present of brucite, the reaction condition led to the formation of HTICs with a

defect structure that make surface area decreasing. After 3^otime reaction, the formation of brucite is detected by XRD and it is obvious that make surface area going back to the fresh.

Catalyst	S _{BET} ^a (m ² /g)	Total NH ₃ uptake normalized S.A. (cm ³ /g)/(m ² /g)	Total CO ₂ uptake normalized S.A. (cm ³ /g)/(m ² /g)
Fresh	237.32	0.0037	0.0618
1 st recycle	173.64	0.0040	0.0939
2 nd recycle	204.07	N.D.	0.0890

a) Determined by nitrogen adsorption using BET technique. **N.D.**) No detected.

Table 7- TPD analysis and physisorption characterization for fresh (5 wt.% Pt/MgAlOx.) and spent catalysts (1^otime reaction and 3^otime reaction)

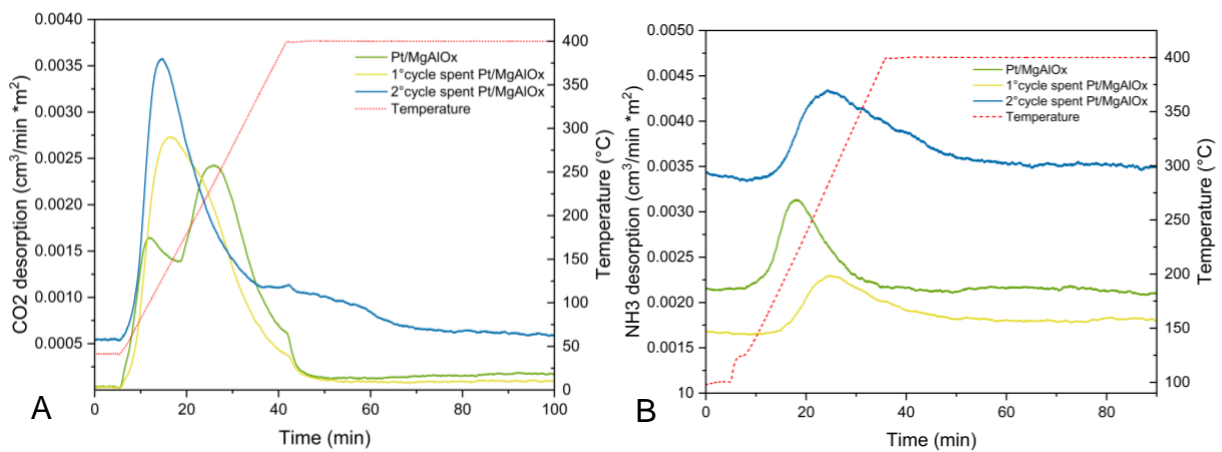


Figure 27- TPD profiles of recycle spent Pt/MgAlOx and fresh Pt/MgAlOx. A) CO₂ desorption and B) NH₃ desorption.

Observing the desorption curves for both analysis we can conclude that the nature of the acid sites doesn't change with the transformation of the mixed oxide to HTICs. On the other hand, the mixed oxide showed 3 different desorption peaks probably

ascribable to different coordinated Mg atoms of the structure of the mixed oxide while after structure transformation only one broad peak is observable because of the coordination of the exposed Mg atoms with hydroxyl groups of the HTlcs structure.

Reaction times	Mg leaching (%)	Al leaching (%)	Pt leaching (%)
1°	6.61	0.00	0.00
2°	4.52	0.00	0.00
3°	2.95	0.00	0.00

Table 8- Element leaching in post-reaction solution.

To exclude a homogeneous activity of the Pt metal through leaching dedicated analysis on the aqueous solution via MP-AES have been performed. The results reported in Table 8 confirmed us that no leaching of both Pt and Al is observable. On the other hand, a ~6.6%wt dissolution of Mg can be clearly observed, this amount tends to decrease over recycle times to a 2.95 %wt in the 3°time reaction mixture. Probably the difference between those two results could be ascribable to the precipitation of brucite $Mg(OH)_2$, visible in the spent catalysts, which seize the Mg from the reaction solution.

5 CONCLUSION:

In conclusion the APR of xylitol aqueous solutions has been investigated optimizing a Pt catalyst supported on a mixed oxide MgAl 3:1. The performance of this catalyst were tested at different reaction conditions and, eventually, an optimized reaction condition of 250°C for 3h reaction time has been found and confirmed. Steps of the reaction mechanism towards retro-aldol reaction of the C5, catalyzed by basic sites of the catalyst, has been verified through APR on glycerol and xylitol under the same conditions due to the detection of common intermediates and similar products distribution. Finally, an in-depth characterization not only on the fresh catalyst but also of the material recovered after reaction (i.e. spent) led us to clearly demonstrate the transformation of the pristine mixed oxide to a HTlcs (LDH) structure which maintain a close-to-constant activity for at least three reaction cycles without any need of reactivation or usage of harsher reaction conditions. More studies should be conducted in future, especially on the liquid phase composition, to understand more in depth the complex reaction mechanism and to be able to use this study for applications on real biomass derived materials, like cellulose, for promoting a really sustainable production of H₂.

6 REFERENCE:

1. Zandalinas, S. I., Fritschi, F. B. & Mittler, R. Global Warming, Climate Change, and Environmental Pollution: Recipe for a Multifactorial Stress Combination Disaster. *Trends Plant Sci.* **26**, 588–599 (2021).
2. CO₂ emissions by fuel or industry type. *Our World in Data* <https://ourworldindata.org/grapher/CO2-by-source>.
3. Glushkov, D. O., Nyashina, G. S., Anand, R. & Strizhak, P. A. Composition of gas produced from the direct combustion and pyrolysis of biomass. *Process Saf. Environ. Prot.* **156**, 43–56 (2021).
4. Manoharan, Y. *et al.* Hydrogen Fuel Cell Vehicles; Current Status and Future Prospect. *Appl. Sci.* **9**, 2296 (2019).
5. Liu, Y., Zhu, Q., Zhang, T., Yan, X. & Duan, R. Analysis of chemical-looping hydrogen production and power generation system driven by solar energy. *Renew. Energy* **154**, 863–874 (2020).
6. Acar, C. & Dincer, I. Review and evaluation of hydrogen production options for better environment. *J. Clean. Prod.* **218**, 835–849 (2019).
7. Liu, W. *et al.* The production and application of hydrogen in steel industry. *Int. J. Hydrog. Energy* **46**, 10548–10569 (2021).
8. Vassilev, S. V., Baxter, D., Andersen, L. K. & Vassileva, C. G. An overview of the chemical composition of biomass. *Fuel* **89**, 913–933 (2010).

9. Zhao, X., Zhang, L. & Liu, D. Biomass recalcitrance. Part I: the chemical compositions and physical structures affecting the enzymatic hydrolysis of lignocellulose. *Biofuels Bioprod. Biorefining* **6**, 465–482 (2012).
10. Maletta, E. & Díaz-Ambrona, C. H. Lignocellulosic Crops as Sustainable Raw Materials for Bioenergy. in *Green Energy to Sustainability* 489–514 (John Wiley & Sons, Ltd, 2020). doi:10.1002/9781119152057.ch20.
11. Tursi, A. A review on biomass: Importance, chemistry, classification, and conversion. *Biofuel Res. J.* **6**, 962–979 (2019).
12. Esposito, D. & Antonietti, M. Redefining biorefinery: the search for unconventional building blocks for materials. *Chem. Soc. Rev.* **44**, 5821–5835 (2015).
13. Ning, P. *et al.* Recent advances in the valorization of plant biomass. *Biotechnol. Biofuels* **14**, 102 (2021).
14. Carpita, N. C. & McCann, M. C. Redesigning plant cell walls for the biomass-based bioeconomy. *J. Biol. Chem.* **295**, 15144–15157 (2020).
15. Cherubini, F. The biorefinery concept: Using biomass instead of oil for producing energy and chemicals. *Energy Convers. Manag.* **51**, 1412–1421 (2010).
16. Anukam, A., Berghel, J., Anukam, A. & Berghel, J. *Biomass Pretreatment and Characterization: A Review. Biotechnological Applications of Biomass* (IntechOpen, 2020). doi:10.5772/intechopen.93607.

17. Chen, H. *et al.* A review on the pretreatment of lignocellulose for high-value chemicals. *Fuel Process. Technol.* **160**, 196–206 (2017).
18. Elangovan, S. *et al.* From Wood to Tetrahydro-2-benzazepines in Three Waste-Free Steps: Modular Synthesis of Biologically Active Lignin-Derived Scaffolds. *ACS Cent. Sci.* **5**, 1707–1716 (2019).
19. Abu-Omar, M. M. *et al.* Guidelines for performing lignin-first biorefining. *Energy Environ. Sci.* **14**, 262–292 (2021).
20. Renders, T., Van den Bossche, G., Vangeel, T., Van Aelst, K. & Sels, B. Reductive catalytic fractionation: state of the art of the lignin-first biorefinery. *Curr. Opin. Biotechnol.* **56**, 193–201 (2019).
21. Renders, T. *et al.* Catalytic lignocellulose biorefining in n-butanol/water: a one-pot approach toward phenolics, polyols, and cellulose. *Green Chem.* **20**, 4607–4619 (2018).
22. Kang, S., Li, X., Fan, J. & Chang, J. Hydrothermal conversion of lignin: A review. *Renew. Sustain. Energy Rev.* **27**, 546–558 (2013).
23. Van den Bosch, S. *et al.* Reductive lignocellulose fractionation into soluble lignin-derived phenolic monomers and dimers and processable carbohydrate pulps. *Energy Environ. Sci.* **8**, 1748–1763 (2015).
24. Cortright, R. D., Davda, R. R. & Dumesic, J. A. Hydrogen from catalytic reforming of biomass-derived hydrocarbons in liquid water. *Nature* **418**, 964–967 (2002).

25. Rinaldi, R. & Schüth, F. Design of solid catalysts for the conversion of biomass. *Energy Environ. Sci.* **2**, 610 (2009).
26. Davda, R. R., Shabaker, J. W., Huber, G. W., Cortright, R. D. & Dumesic, J. A. A review of catalytic issues and process conditions for renewable hydrogen and alkanes by aqueous-phase reforming of oxygenated hydrocarbons over supported metal catalysts. *Appl. Catal. B Environ.* **56**, 171–186 (2005).
27. Chheda, J. N., Huber, G. W. & Dumesic, J. A. Liquid-Phase Catalytic Processing of Biomass-Derived Oxygenated Hydrocarbons to Fuels and Chemicals. *Angew. Chem. Int. Ed.* **46**, 7164–7183 (2007).
28. Coronado, I. *et al.* A review of catalytic aqueous-phase reforming of oxygenated hydrocarbons derived from biorefinery water fractions. *Int. J. Hydrog. Energy* **41**, 11003–11032 (2016).
29. Wei, Y. *et al.* Renewable Hydrogen Produced from Different Renewable Feedstock by Aqueous-Phase Reforming Process. *J. Sustain. Bioenergy Syst.* **04**, 113–127 (2014).
30. Kirilin, A. V. *et al.* Aqueous phase reforming of xylitol and sorbitol: Comparison and influence of substrate structure. *Appl. Catal. Gen.* **435–436**, 172–180 (2012).
31. Kechagiopoulos, P. N., Voutetakis, S. S., Lemonidou, A. A. & Vasalos, I. A. Hydrogen Production via Steam Reforming of the Aqueous Phase of Bio-Oil in a Fixed Bed Reactor. *Energy Fuels* **20**, 2155–2163 (2006).

32. Pipitone, G., Zoppi, G., Pirone, R. & Bensaid, S. A critical review on catalyst design for aqueous phase reforming. *Int. J. Hydrog. Energy* **47**, 151–180 (2022).
33. Kim, Y. *et al.* High purity hydrogen production via aqueous phase reforming of xylose over small Pt nanoparticles on a γ -Al₂O₃ support. *Int. J. Hydrog. Energy* **45**, 13848–13861 (2020).
34. Grenoble, D. C., Estadt, M. M. & Ollis, D. F. The chemistry and catalysis of the water gas shift reaction: 1. The kinetics over supported metal catalysts. *J. Catal.* **67**, 90–102 (1981).
35. Vannice, M. A. The catalytic synthesis of hydrocarbons from H₂CO mixtures over the Group VIII metals: V. The catalytic behavior of silica-supported metals. *J. Catal.* **50**, 228–236 (1977).
36. Pipitone, G. *et al.* Aqueous phase reforming of sugar-based biorefinery streams: from the simplicity of model compounds to the complexity of real feeds. *Catal. Today* **345**, 267–279 (2020).
37. Bugli, F. Valorizzazione di idrolizzati da cellulosa tramite catalisi eterogenea. (University of Bologna, 2017).
38. Cabezón, M. I. A. Aqueous phase reforming of renewables for hydrogen production in presence of supported platinum and palladium catalysts. 89.
39. Fasolini, A., Cespi, D., Tabanelli, T., Cucciniello, R. & Cavani, F. Hydrogen from Renewables: A Case Study of Glycerol Reforming. *Catalysts* **9**, 722 (2019).

40. Fasolini, A., Cucciniello, R., Paone, E., Mauriello, F. & Tabanelli, T. A Short Overview on the Hydrogen Production Via Aqueous Phase Reforming (APR) of Cellulose, C6-C5 Sugars and Polyols. *Catalysts* **9**, 917 (2019).
41. Li, N. & Huber, G. W. Aqueous-phase hydrodeoxygenation of sorbitol with Pt/SiO₂-Al₂O₃: Identification of reaction intermediates. *J. Catal.* **270**, 48–59 (2010).
42. Tabanelli, T., Bugli, F, Longo, S. & Nascetti, D. Catalizzatore magnetico per il frazionamento catalitico riduttivo di biomasse lignocellulosiche. (2021). Application number: 102021000005024, filing date: 4th March 2021. Applicants Hera SpA and University of Bologna.
43. Xia, Q. *et al.* Catalytic Deoxygenation of Xylitol to Renewable Chemicals: Advances on Catalyst Design and Mechanistic Studies. *Chem. Rec.* **21**, 133–148 (2021).
44. Xiong, M., Gao, Z. & Qin, Y. Spillover in Heterogeneous Catalysis: New Insights and Opportunities. *ACS Catal.* **11**, 3159–3172 (2021).
45. Shokrollahi, H. A review of the magnetic properties, synthesis methods and applications of maghemite. *J. Magn. Magn. Mater.* **426**, 74–81 (2017).
46. Kim, W. *et al.* A new method for the identification and quantification of magnetite–maghemite mixture using conventional X-ray diffraction technique. *Talanta* **94**, 348–352 (2012).

47. Soares, A. V.-H., Perez, G. & Passos, F. B. Alumina supported bimetallic Pt–Fe catalysts applied to glycerol hydrogenolysis and aqueous phase reforming. *Appl. Catal. B Environ.* **185**, 77–87 (2016).
48. Guo, Y., Azmat, M. U., Liu, X., Wang, Y. & Lu, G. Effect of support's basic properties on hydrogen production in aqueous-phase reforming of glycerol and correlation between WGS and APR. *Appl. Energy* **92**, 218–223 (2012).
49. Bobadilla, L. F., Penkova, A., Romero-Sarria, F., Centeno, M. A. & Odriozola, J. A. Influence of the acid–base properties over NiSn/MgO–Al₂O₃ catalysts in the hydrogen production from glycerol steam reforming. *Int. J. Hydrog. Energy* **39**, 5704–5712 (2014).
50. Larimi, A. S., Kazemeini, M. & Khorasheh, F. Highly selective doped PtMgO nano-sheets for renewable hydrogen production from APR of glycerol. *Int. J. Hydrog. Energy* **41**, 17390–17398 (2016).
51. Shen, J., Kobe, J. M., Chen, Y. & Dumesic, J. A. Synthesis and Surface Acid/Base Properties of Magnesium-Aluminum Mixed Oxides Obtained from Hydrotalcites. *Langmuir* **10**, 3902–3908 (1994).
52. Lombardi, E. Catalytic aqueous phase conversion of polyols to hydrogen and chemicals. (University of Bologna, 2017).
53. Angyal, S. J. The Lobry de Bruyn-Alberda van Ekenstein Transformation and Related Reactions. in *Glycoscience: Epimerisation, Isomerisation and*

Rearrangement Reactions of Carbohydrates (ed. Stütz, A. E.) 1–14 (Springer, 2001). doi:10.1007/3-540-44422-X_1.

54. Hausoul, P. J. C., Beine, A. K., Neghadar, L. & Palkovits, R. Kinetics study of the Ru/C-catalysed hydrogenolysis of polyols – insight into the interactions with the metal surface. *Catal. Sci. Technol.* **7**, 56–63 (2017).
55. Pérez-Ramírez, J., Abelló, S. & van der Pers, N. M. Memory Effect of Activated Mg–Al Hydrotalcite: In Situ XRD Studies during Decomposition and Gas-Phase Reconstruction. *Chem. – Eur. J.* **13**, 870–878 (2007).
56. López-Asensio, R. *et al.* Mixed Oxides Derived from Hydrotalcites Mg/Al Active in the Catalytic Transfer Hydrogenation of Furfural to Furfuryl Alcohol. *Catalysts* **13**, 45 (2022).
57. Kwon, S. *et al.* CO₂ Sorption. in *Coal Gasification and Its Applications* 293–339 (Elsevier, 2011). doi:10.1016/B978-0-8155-2049-8.10010-5.